Spectrochimica Acta Part A: Molecular and Biomolecular Spectroscopy 256 (2021) 119709

Contents lists available at ScienceDirect

Spectrochimica Acta Part A: Molecular and Biomolecular Spectroscopy

journal homepage: www.elsevier.com/locate/saa

Luminescent lanthanide(III) complexes of DTPA-bis(amido-phenyl-terpyridine) for bioimaging and phototherapeutic applications

Srikanth Dasari [a], Swati Singh [b], Zafar Abbas [a], Sri Sivakumar [b], Ashis K. Patra [a,*]

[a] Department of Chemistry, Indian Institute of Technology Kanpur, Kanpur 208016, UP, India
[b] Department of Chemical Engineering and Center for Environmental Science and Engineering, Indian Institute of Technology Kanpur, Kanpur 208016, UP, India

HIGHLIGHTS

- A series of [Ln(dtntp)(H_2O)] (**1**–**5**) complexes were synthesized as cell imaging and phototherapeutic agents.
- The pendant phenyl-terpyridine (Ph-tpy) moieties act as photo-sensitizing antennae to impart the desirable optical properties.
- The luminescence of Eu(III) and Tb (III) used for fluorescence imaging studies.
- Eu(III) and Tb(III) complexes show photocytotoxicity in HeLa cells at 365 nm.

GRAPHICAL ABSTRACT

A series of coordinatively saturated and thermodynamically stable [Ln(dtntp)(H_2O)] (**1**–**5**) bioprobes were synthesized utilizing strategically designed novel DTPA-bisamide ph-tpy (**dtntp)** ligand, to satisfy and modulate the dual functional prerequisites as cellular imaging and phototherapeutic agents.

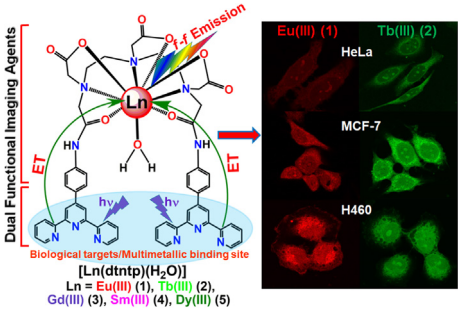

ARTICLE INFO

Article history:
Received 17 October 2020
Received in revised form 31 January 2021
Accepted 10 March 2021
Available online 18 March 2021

Keywords:
Lanthanide
Luminescence
Europium
Terbium
DTPA
Bioimaging
Photocytotoxicity

ABSTRACT

We report here a series of coordinatively-saturated and thermodynamically stable luminescent [Ln(dtntp)(H_2O)] [Ln(III) = Eu (**1**), Tb (**2**), Gd (**3**), Sm (**4**) and Dy (**5**)] complexes using an aminophenyl-terpyridine appended-DTPA (**dtntp)** chelating ligand as cell imaging and photocytotoxic agents. The *N, N″*-bisamide derivative of H_5DTPA named as **dtntp** is based on 4′-(4-aminophenyl)-2,2′:6′,2″-terpyridine conjugated to diethylenetriamine-*N,N′,N″*-pentaacetic acid. The structure, physicochemical properties, detailed photophysical aspects, interaction with DNA and serum proteins, and photocytotoxicity were studied. The intrinsic luminescence of Eu(III) and Tb(III) complexes due to f → f transitions used to evaluate their cellular uptake and distribution in cancer cells. The solid-state structure of [Eu(dtntp)(DMF)] (**1**·DMF) shows a discrete mononuclear molecule with nine-coordinated {EuN_3O_6} distorted tricapped-trigonal prism (TTP) coordination geometry around the Eu(III). The {EuN_3O_6} core results from three nitrogen atoms and three carboxylate oxygen atoms, and two carbonyl oxygen atoms of the amide groups of dtntp ligand. The ninth coordination site is occupied by an oxygen atom of DMF as a solvent from crystallization. The designed probes have two aromatic pendant phenyl-terpyridine (Ph-tpy) moieties as photo-sensitizing antennae to impart the desirable optical properties for cellular imaging and photocytotoxicity. The photostability, coordinative saturation, and energetically rightly poised triplet states of dtntp ligand allow the efficient energy transfer (ET) from Ph-tpy to the emissive excited states of the Eu(III)/Tb(III), makes them luminescent cellular imaging probes. The Ln(III) complexes show significant binding tendency to DNA ($K \sim 10^4\ M^{-1}$), and serum proteins (BSA and HSA) ($K \sim 10^5\ M^{-1}$). The luminescent Eu(III) (**1**) and Tb(III) (**2**) complexes were utilized for cellular internalization and cytotoxicity studies due to their optimal photophysical properties. The cellular uptake studies using fluorescence

* Corresponding author.
E-mail address: akpatra@iitk.ac.in (A.K. Patra).

https://doi.org/10.1016/j.saa.2021.119709
1386-1425/© 2021 Published by Elsevier B.V.

imaging displayed intracellular (cytosolic and nuclear) localization in cancer cells. The complexes **1** and **2** displayed significant photocytotoxicity in HeLa cells. These results offer a modular design strategy with further scope to utilize appended *N,N,N*-donor tpy moiety for developing light-responsive luminescent Ln (III) bioprobes for theranostic applications.

© 2021 Published by Elsevier B.V.

1. Introduction

Designing of lanthanide probes for biomedical applications have been gaining great attention in recent decades, e.g. as MRI contrast agents in medical diagnosis and therapy, biomarkers for immunoassays, photodynamic therapy (PDT), bioimaging and multimodal imaging agents [1–6]. Magnetic resonance imaging (MRI) is a popular imaging technique in medical diagnostics and biomedical imaging. In MRI, thermodynamically stable Gd(III)-based acyclic diethylenetriaminepentaacetic acid ($[Gd(DTPA)(H_2O)]^{2-}$, Magnevist®) and the cyclic 1,4,7,10-tetraazacyclododecane-1,4,7,10-tetraacetic acid ($[Gd(DOTA)(H_2O)]^{-}$, Dotarem®)[7] complexes are the most widespread MRI contrast agents in clinical use. Luminescent Ln(III) probes coupled with MRI improves the diagnostic ability in multimodal imaging [8–10].

Ln(III) complexes with multidentate ligands, viz. DTPA, DOTA, cyclen derivative were well exploited as MRI contrast agents, bioimaging, cellular staining, or theranostic applications [3–5,9–13]. This is due to their excellent thermodynamic stability originated from multidentate chelating ligands. The unique optical properties like large Stokes' shifts, line-like emission bands, longer lifetime (ms–μs), higher quantum yields are highly suitable for interference-free *invitro* and *invivo* cellular imaging applications. The time-resolved luminescence coupled microscopic techniques with high S/N ratio allows possible real-time imaging using long-lived Ln(III) probes, and eliminates the short-lived autofluorescence from indigenous biological fluorophores [11-14]. The DTPA-bisamide based multidentate chelates with eight coordination sites forms coordinatively-saturated and thermodynamically stable Ln(III) complexes. These scafoldes protect the emissive Ln (III) from nonradiative vibrational energy dissipation for bioimaging and sensing applications [3–5]. Thus, design of Ln(III) probes with multidentate ligands like DTPA or DOTA, appended with light harvesting fluorophore in single platform is a strategic approach for the design of highly luminescent lanthanide-based bioprobes [1–5,11–14].

One of the emerging applications of Ln(III) complexes is in photodynamic therapy (PDT) and light-responsive theranostic agents [15,16]. Ln(III) probes with photosensitizing antenna act as multimodal phototherapeutic agents considering favorable intersystem crossing (ISC) due to heavy-atom effect. This results in facile generation $^1O_2$/ROS, which ultimately leads to apoptotic cell death [16,17]. Moreover, recently lanthanide-based upconversion nanoparticles (UCNP) were elegantly used in imaging-guided phototherapy [18]. The Yb,Er-UCNPs with excellent depth of penetration of NIR radiation, transparent biological window, and biocompatibility are ideal choice for non-invasive PDT modality. Ln(III) probes also avoid the drawbacks (prolonged skin sensitivity and hepatotoxicity) of conventional porphyrin-based PDT agents [16a-b]. Recently, K.-L. Wong et al., strategically designed Ln(III) probes as new-generation PDT agent, light-triggered delivery and tracking of anticancer drugs and as imaging probes for the early prognosis of disease biomarkers [17,19].

The present work emerges from our continuousinterest in exploring and designing stable luminescent lanthanide complexes for bioimaging and theranostic applications [20,21]. In the previous works, we reported several Ln(III) complexes with bidentate *N,N*-donor (e.g., dipyridoquinoxaline, dpq; dipyridophenazine, dppz) or *O,O*-donor β-diketonates (e.g. (trifluoro-1-(2-naphthyl)-1,3-butanedionate, tfnb; thenoyltrifluoroacetone, ttfa) ligands. These complexes can acts as effective luminescent bioprobes for cellular imaging and phototherapeutic agents in the visible to NIR region [20]. However, these Ln(III) probes have some intrinsic limitations like the necessity of secondary ligands to fulfill the coordination sphere for desirable thermodynamic stability and poor aqueous solubility. We attempt here to overcome some of these limitations associated with these probes and to fulfill the necessary criteria to develop efficient luminescent Ln(III) probes. Herein, we have designed a new multidentate poly(aminocarboxylate) chelator (**dtntp**) based on DTPA-functionalized with 4′-(4-aminophenyl)-2,2′:6′,2″-terpyridine moiety as light-harvesting pendant antenna, as well to form thermodynamically stable lanthanide complexes. We elegantly utilized **dtntp** ligand for designing stable luminescent $[Ln(dtntp)(H_2O)]$ (Ln(III) = Eu (**1**), Tb (**2**), Gd (**3**), Sm (**4**) and Dy (**5**)) complexes to modulate the desirable optical properties for cellular imaging application (Scheme 1). [Eu(dtntp)(DMF)] (**1**·DMF) was structurally characterized and reveals a nine-coordinate $\{EuN_3O_6\}$ tricapped-trigonal prismatic (TTP) coordination geometry around the Eu(III). The dtntp ligand here serves multiple purposes: (i) it provides eight coordination sites and forms strong complexation with the Ln(III) with high thermodynamic stability; (ii) protects the Ln(III) ion from nonradiative vibrational or solvent quenching; (iii) the pendant ph-tpy antenna facilitate efficient ET to the Ln(III) ions to generate the emissive excited states which results in enhanced luminescence intensity; (iv) the pendant phenyl-terpyridine moieties on dtntp are capable to generate photo-induced $^3(\pi\text{-}\pi^*)$ and/or $^3(n\text{-}\pi^*)$ excited states to transfer their energy to $^3O_2$ to form ROS that causes the cell death [20,21]. Ln(III) complexes are showing significant DNA and protein binding propensity due to planer terpyridine moieties which can intercalate with DNA and serum proteins. The intrinsic red and green luminescence of the Eu(III) (**1**) and Tb(III) (**2**) were utilized for cellular imaging studies in HeLa, MCF-7 and H460 cancer cells using confocal fluorescence microscopy. The complexes **1** and **2** display significant photocytotoxicity at 365 nm UV-A light. Overall, present study offer a modular strategy to satisfy the essential criteria for designing Ln(III) probes for multimodal imaging and phototherapeutic agents.

2. Results and discussion

2.1. Synthesis and general aspects

The dtntp ligand was synthesized by reacting two equivalents of 4′-(4-aminophenyl)-2,2′:6′,2″-terpyridine with diethylenetriamine-*N,N′,N″*-pentaacetic acid (DTPA)-bis-anhydride in dry DMF resulting in ~87% yield (Scheme 2). The free ligand was characterized by ESI-MS and FT-IR (Fig. S1). The (+)-ion mode ESI-MS spectra of the **dtntp** showed the molecular ion peak $[M+H]^+$ at *m*/*z* 1006.40. The FT-IR spectra show strong absorption band at 1665 cm^{-1} attributed to the $\nu_{C=O}$ of the free acid, while the bands at 1601 cm^{-1} and 1585 cm^{-1} correspond to ($\nu_{CONH\text{-}}$) of amides. The broad band around 3414 cm^{-1} corresponds to $\nu_{N\text{-}H}$ or $\nu_{O\text{-}H}$ of the dtntp ligand [22,23]. The $[Ln(dtntp)((H_2O)]$ (Ln

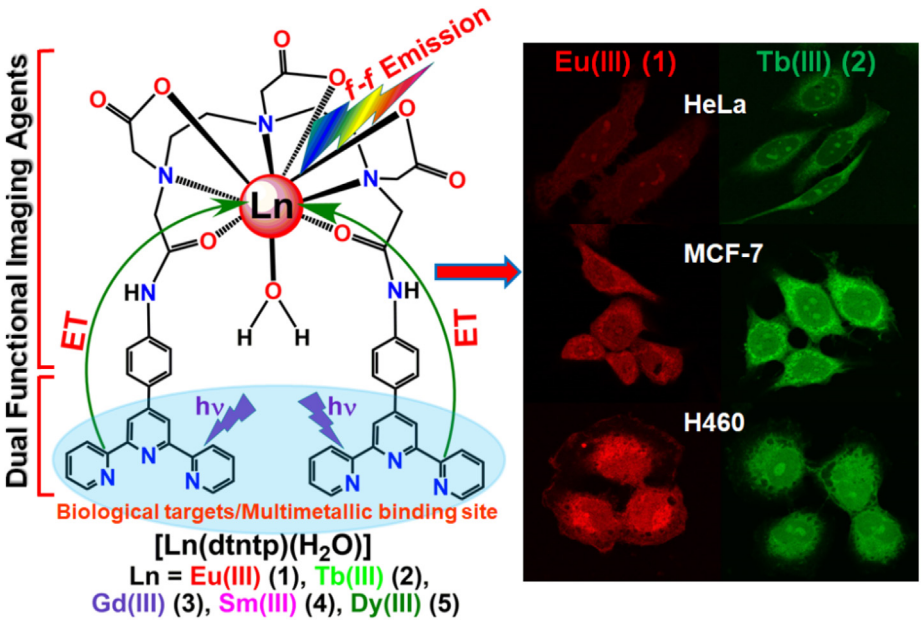

Scheme 1. The design strategy for [Ln(dtntp)(H_2O)] (**1**–**5**) bioprobes containing photosensitizing dtntp pendant antenna moiety for bioimaging and phototherapeutic applications.

(III) = Eu (**1**), Tb (**2**), Gd (**3**), Sm (**4**), Dy (**5**)) complexes were synthesized following a generalized synthetic route (Scheme 2), with ~84% yield by reacting Eu/Tb(CF_3SO_3)$_3$, Gd(NO_3)$_3$·6H_2O, Dy(NO_3)$_3$·hydrate and $SmCl_3$·6H_2O with 1:1 mol ratio of dtntp^{3-} deprotonated by NaOH in 1:3 mol ratio with the free ligand, in boiling methanol. The ESI-MS spectra of the complexes **1**–**4** showed respective molecular ion peaks as [M−H_2O + H]$^+$. The complex **5** shows *m*/*z* peak for [M−H_2O]$^+$ with predicted isotopic distribution (Figs. S2-S6). The presence of molecular ion peaks in ESI-MS displaying incorporation of respective Ln(III) in the dtntp core and their structural integrity in solution. However, in aqueous-DMF solution, presumably, there will be fast ligand-exchange reactions between DMF and water as determined by inner-sphere hydration number (*q*) values of the compounds due to fast ligand-exchange kinetics of Ln(III). Upon complexation, the FT-IR spectra of the complexes showed lower $\nu_{C=O}$ stretching (~60 cm^{-1}) compared to free dtntp ligand, which suggests oxygen coordination to the Ln (III) ions. The overlapping FT-IR spectra of the complexes suggest their structural resemblances (Figure S7). These results are consistent with the previously reported analogous nine-coordinated DTPA–bisamide derivatives with lanthanides. Here Ln(III) ion is coordinated to **dtntp** via three oxygen atoms of the carboxylate groups and three nitrogen atoms and two carbonyl oxygen atoms of the amide groups, and the ninth coordination site is occupied by a water molecule [21–25]. The solid-state structure of [Eu(dtntp)(DMF)] (**1**) also confirms this bonding connectivity in a nine-coordinated TTP geometry.

2.2. X-ray crystal structure

The single crystals of complex **1** were obtained from the layering of Et_2O into a DMF/methanol solution of complex **1** at RT. The X-ray structure shows discrete mononuclear nine coordination {EuN_3O_6} polyhedra around the Eu(III) center. It crystallized in the triclinic space group *P*-1 with eight molecules in the unit cell. The asymmetric unit contains one MeOH as a solvent of crystallization. The Eu(III) complex has one bound DMF on the ninth coordination site as a solvent of crystallization.

The selected crystallographic data and bonding parameters for complex **1** were shown in Table S1. The ORTEP diagram of complex

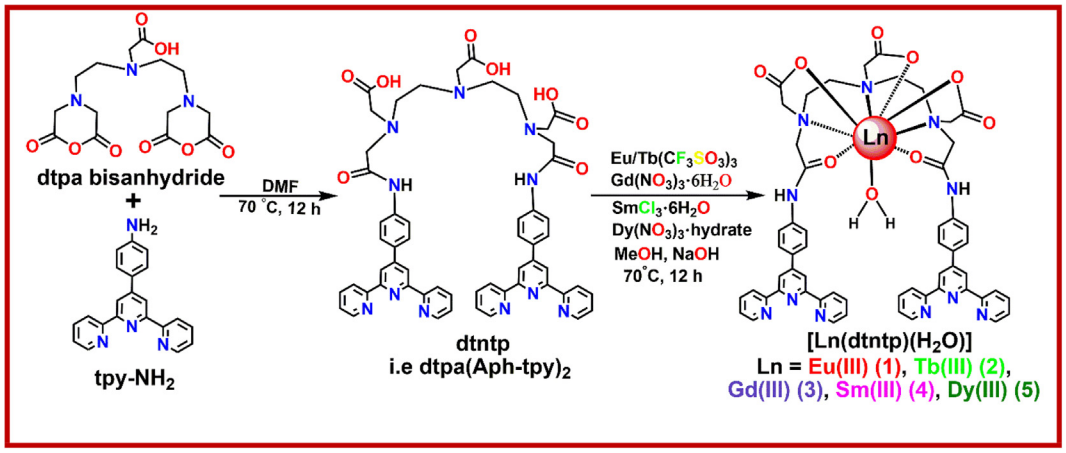

Scheme 2. Synthesis of the dtntp ligand and [Ln(dpntp)(H_2O)] complexes (Ln(III) = Eu (**1**), Tb (**2**), Gd (**3**), Sm (**4**), Dy (**5**).

1 is given in Fig. 1a. The unit cell packing diagram is shown in Figure S8, and selected bond lengths and bond angles reported in Table S2. The Eu(III) is coordinated through the three carboxylate oxygens, two amide oxygens, and three amine nitrogens of the eight-coordinated dtntp chelator. The ninth coordination site is occupied by the oxygen atom of the DMF solvent used for crystallization. Such coordination results in a nine-coordinated $\{EuN_3O_6\}$ distorted tricapped-trigonal prism (TTP) geometry around the Eu (III) center (Fig. 1b) [24,26–29]. The terminal amine nitrogens (N1, N2) together with the O9 oxygen of the coordinated DMF, are forming the three rectangular face caps. The two triangular faces of the trigonal prism are constituted by a pair of [O1, O2, O5] and [N3, O3, O4] set of planes, respectively. The Eu(III) is sitting in the middle of the trigonal prism, and Eu–$O(9)_{DMF}$ bond is almost protruding out perpendicularly to the rectangular mean plane to which it's capped. Eu–O_{amide} bond distances range from 2.480(3) Å to 2.452(4) Å and Eu–$O_{carboxylate}$ bond length ranges from 2.386 (3) Å to 2.352(3) Å. Eu-$N_{terminal}$ bonds range from 2.740(4) Å to 2.641(3) Å, whereas Eu-$N_{central}$ bond length is 2.643(3) Å and Ln-O_{DMF} bond distance is 2.417(3) Å respectively, which are comparable with the literature reported values [24,26–29]. On average, Eu–N bond distances are ~0.3 Å longer than the Eu–O distances revealing the higher bond strength of the Eu–O ionic bonds, as compared to the less polar Ln–N bonds [24,26–29]. We presume analogous isostructures for other [Ln(dtntp)(Solv)] compounds, as observed earlier with related DTPA-bisamide-quinoline derivatives, considering similar binding modes for Ln(III) [24a].

2.3. Photophysical properties

UV–visible absorption spectra of the ligand and the Ln(III) complexes **1**–**5** in aqueous-DMF (99: 1 v/v) shows broad bands in the range of ~270 to 350 nm with absorption maxima at 284 nm and a broad shoulder at 324 nm can be attributed to the ligand-centered π-π^* and n-π^* electronic transition of DTPA-bis-amide-phenyl-terpyridine based dtntp ligand (Fig. 2a) [22–24]. The significant resemblance of the UV–visible spectra of the Ln(III) complexes **1**–**5** suggests electronic states are quite independent of the nature of Ln(III) and very minimal ligand-field effect. The excitation spectra for the complexes **1**–**5** were recorded using their most intense Ln(III) emission bands. The excitation spectra in Fig. 2b show broad bands ranging from ~270 to 350 nm, which resembles their absorption spectra, which indicates, the Ln(III) emission is sensitized through the photosensitizing pendant ph-tpy antenna [22,23]. The time-dependent absorption spectral traces for the complexes **1**–**5** in aqueous-DMF and in Tris buffer at 298 K do not show any noticeable changes. This suggests the complexes' excellent thermodynamic stability in solution as dtntp chelate forms coordinatively saturated stable lanthanide complexes.

The efficient energy transfer (ET) requires a suitable energy difference between the triplet state (^3T) of the sensitizing antenna and the emissive excited states of the Ln(III) ions. An optimal L → Ln(III) ET-process depends on ligands, which is capable of effective energy transfer to its triplet state via intersystem crossing (ISC). The desirable energy gap (ΔE) between the lowest triplet states of ligands (e.g., ^3n-π^*, $^3\pi$-π^*) to the emissive excited states of Ln(III) ideally $\geq$ 2500 cm^{-1} according to the Latva'a empirical rule [20,30,31].

To gain more insights into the energy gap of Ln(III) and ligand triplet states, we measured the photophysical properties of the dtntp ligand and Gd(III) complex (**3**) in aqueous-DMF at 298 K shown in the Figs. S9-S10. The steady-state luminescence spectra of Gd(III) complex at λ_{ex} = 284 nm results in ligand-centered broad emission that arises mainly from singlet states ($^1\pi$–π^*) (Fig. S10). The phosphorescence mode spectra of Gd(III) complex showing the lower energy triplet states ($^3\pi$–π^*) emission, which is independent of the ligand to Gd(III) energy transfer. The Gd(III) emissive excited state ($^6P_{7/2}$) situated much higher in energy than the dtntp, thus arrest any ligand-to-metal energy transfer. As a result, the detected luminescence is exclusively due to the dtntp chromophore, which further allows us to determine the triplet state (T_1) energy of the dtntp ligand [22,31]. To estimate the approximate energy transfers pathways (due to only available room temperature data) in the Ln(III) complexes, the approximate singlet (S_1) and triplet (T_1) energy levels of the dtntp ligand (324 nm, 30864 cm^{-1}, and 410 nm, 24400 cm^{-1}) were obtained by referencing their higher absorption edges and lower emission edge wavelengths of the corresponding phosphorescence spectra of dtntp ligand and [Gd(dtntp)(H_2O)] (**3**) at 298 K [20–23]. The $^5D_0$ emissive excited states of Eu(III) (17500 cm^{-1}), $^5D_4$ of Tb(III) (20400 cm^{-1}), $^4G_{5/2}$ of Sm(III) (17800 cm^{-1}) and $^4F_{15/2}$ state of Dy(III) (21000 cm^{-1}) are well-known and obtained from the literature [32,33]. We determined the approximate qualitative energy gap (ΔE = E_{T1}-E_{Ln^*}) between the T_1 state of dtntp ligand and excited-state energy levels of the Eu(III) (ΔE ~ 6900 cm^{-1}), Tb(III) (ΔE ~ 4000 cm^{-1}), Sm(III) (ΔE ~ 6600 cm^{-1}) and Dy(III) (ΔE ~ 3400 cm^{-1}) respectively at RT from photoluminescence and phosphorescence measurements. The determined room-temperature T_1 state energy level of the dtntp ligand is at higher

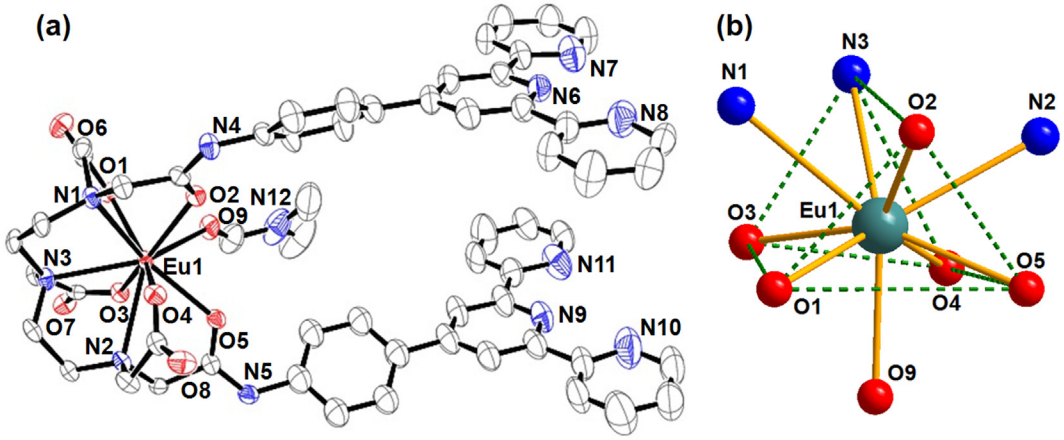

Fig. 1. (a) ORTEP view of [Eu(dtntp)(DMF)] (**1**·DMF) at 50% probability thermal ellipsoid with the heteroatom numbering scheme. The hydrogen atoms were omitted for clarity. (b) Coordination polyhedra of (**1**) showing the nine-coordinate $\{EuN_3O_6\}$ Eu(III) core with distorted tricapped-trigonal prism (TTP) coordination geometry.

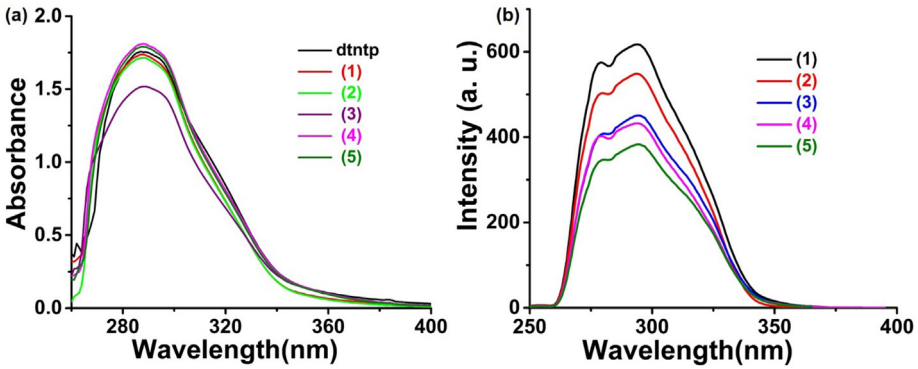

Fig. 2. (a) UV–vis absorption spectra of dtntp and [Ln(dtntp)(H_2O)] complexes **1**–**5** (28 μM) in aqueous-DMF (1:99, %DMF: %H_2O) at 298 K. (b) Excitation spectra of complexes **1**–**5** (10 μM) in aqueous-DMF (1:99, %DMF: %H_2O) at 298 K, (λ_{em} = 615 nm (**1**), λ_{em} = 545 nm (**2**), λ_{em} = 410 nm (**3**), λ_{em} = 598 nm (**4**), λ_{em} = 570 nm (**5**), Exc. and Em. slit width = 5 nm.

energy than the emissive excited states of the Ln(III) ions. The approximate schematic energy level diagram with possible intramolecular ET process from dtntp antenna to the emissive excited state of Ln(III) was shown in Fig. 3. In complexes **1** and **2**, this energy difference is sufficiently higher, which facilitates the efficient ET from the pendant dtntp antenna triplet state to the emissive excited states ($^5D_0$) of Eu(III) and ($^5D_4$) of Tb(III). However, such indirect energy transfer to the excited states of Sm(III) ($^4G_{5/2}$) and of Dy(III) ($^4F_{15/2}$) was found less effective as observed from their weak luminescence properties. A more precise quantitative understanding of energy-levels requires low-temperature (e.g., Liquid N_2, 77 K) phosphorescence measurements along with theoretical calculation of the associated energy levels.

The time-resolved luminescence spectra of the complexes **1** and **2** upon excitation at 284 nm, display intrinsic red and green luminescence of Eu(III) and Tb(III) due to $^5D_0 \rightarrow {}^7F_J$ (J = 0–4) and $^5D_4 \rightarrow {}^7F_J$ (J = 6–3) transitions respectively (Fig. 4). The excited-state luminescent lifetimes of Eu(III) (**1**) and Tb(III) (**2**) was measured in the H_2O and D_2O at room temperature to determine the number of Ln(III)-coordinated water molecules in aqueous media (Table 1). The emission decay profiles were fitted by using a single-exponential fitting (Fig. S13). The hydration number (q) for complexes **1** and **2** was calculated using the modified Horrocks' equation [34]. The determined q values for the Ln(III) complexes q_{Eu} = 1.2 (**1**) and q_{Tb} = 1.1 (**2**) confirms the presence of one coordinated water molecule. This is in good agreement with the solid-state structure of [Eu(dtntp)(DMF)] (**1**·DMF), which contains only one labile and exchangeable coordinated DMF molecule. These q values are consistent with the literature reported nine-coordinated lanthanide complexes with DTPA-bisamide derivatives; those generally provide eight coordination sites to the Ln(III), and the ninth coordination site is occupied by one water molecule in aqueous media [21a,23,28,29].

The Sm(III) (**4**) and Dy(III) (**5**) complexes at λ_{ex} = 284 nm showed characteristic visible emission bands for Sm(III) and Dy (III) ions, attributed to $^4G_{5/2} \rightarrow {}^6H_J$ (J = 5/2 → 13/2) and $^4F_{15/2}/{}^4F_{9/2} \rightarrow {}^6H_J$ (J = 15/2 → 9/2) f–f transitions (Fig. 5) [32c-32f]. The presence of ligand-based fluorescence observed at ~410 nm in complexes **4** and **5** implies that the energy transfer from **dtntp** to Sm(III) and Dy (III) is not optimal with poor quantum yields [22–23,32]. The monoexponential decay curves presumably indicating the presence of a single chemical environment (i.e. exchange of one labile ligand-exchange site) around each luminescent Ln(III) ion in the solution (Fig. S14, Table 1) [21–24].

The overall quantum yield ($\Phi_{overall}$) of the complexes **1**–**5** were measured in the H_2O, and D_2O reported in the Table 1 are comparable or higher than the existing Ln(III) complexes with DTPA-bis amide derivatives [31–35]. As compared to complexes **1** and **2**,

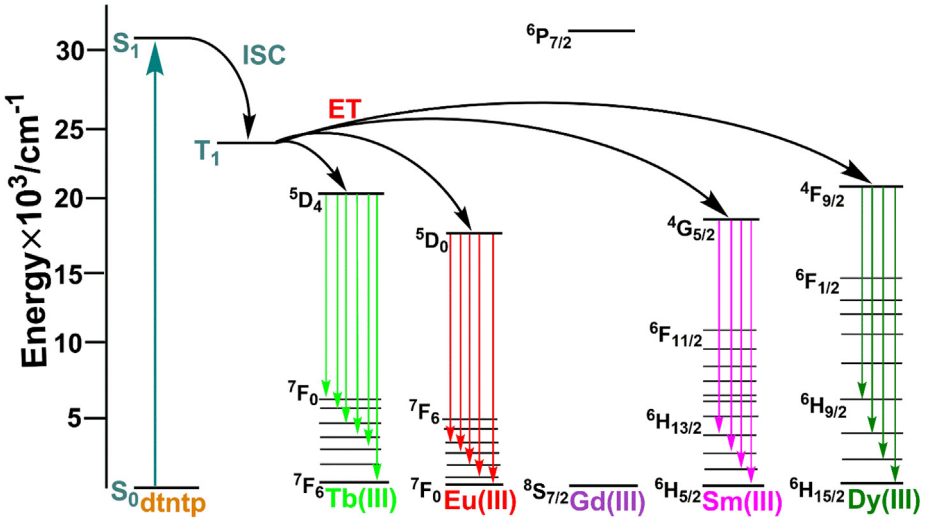

Fig. 3. Schematic approximate energy level diagram showing the possible intramolecular energy transfer processes from **dtntp** antenna to the emissive excited states of Ln (III) in complexes **1**–**5** based on photophysical data at 298 K. S_1, first excited singlet state; T_1, first excited triplet state, *ISC*, intersystem crossing.

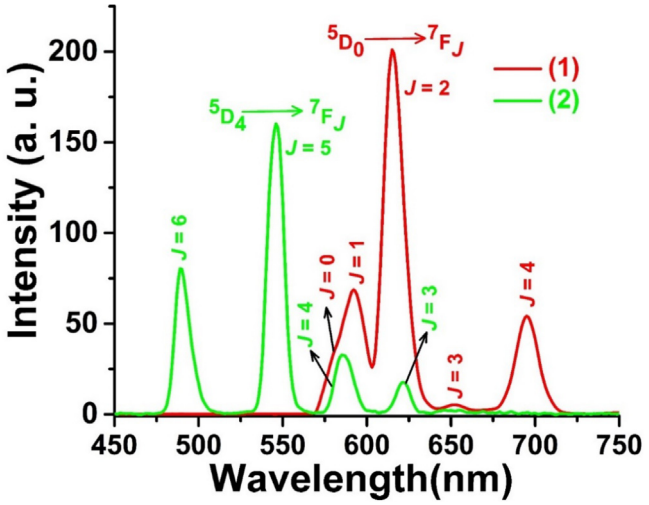

Fig. 4. Time-resolved luminescence spectra of complexes **1** (red) and **2** (green) in aqueous-DMF (1:99, %DMF: %H_2O) showing their corresponding $^5D_0/^5D_4 \rightarrow {}^7F_J$ transitions. ([complex] = 12 μM, λ_{ex} = 284 nm, Exc./Em. slit width = 5 nm).

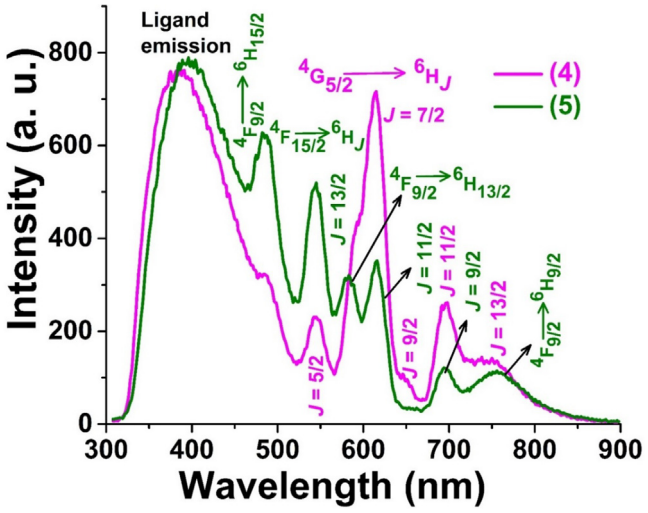

Fig. 5. Luminescence spectra of complexes **4** (magenta) and **5** (olive) in aqueous-DMF (1:99, %DMF: %H_2O) showing their corresponding $^4G_{5/2}$ and $^4F_{15/2}/^4F_{9/2} \rightarrow {}^6H_J$ transitions. (20 μM, λ_{ex} = 284 nm, Exc./Em. slit width = 10 nm).

the lower τ and Φ of the complexes **4** and **5** are mainly due to the Sm(III) and Dy(III) excited states are more susceptible towards additional non-radiative deactivation pathways. Their excited states are possibly quenched by non-radiative vibrational relaxation by O–H and N–H oscillators present in the surrounding solvent and ligand [22a, 35]. The stuided Ln(III) complexes follow similar trend in excited state lifetimes (τ) and overall quantum yield (Φ) with analogous Ln(III)- DTPA-bis amide derivatives. For example, for Ln(III)- DTPA-bis-6-aminoquinoline (LnL) (τ and Φ for EuL = 0.6 ms and 4%; SmL = 0.01 ms, 0.1%) [22a]. Similar trend in $\Phi_{overall}$ observed in a series of Ln(III) complexes with DTPA-bis-*p*-thiophenyl derivatives (LnL^x) (Φ = EuL^x, TbL^x, DyL^x and SmL^x are 0.32%, 0.04%, 0.03% and 0.02% respectively) [35a].

The longer τ and higher Φ of the complexes in D_2O as compared to H_2O is the results of less nonradiative deactivation induced by O–D vibrations than by O–H [36]. Overall, the present series of Ln(III) complexes show higher thermodynamic stability, coordinative saturation (q = 1), desirable optical parameters, photostability. These properties underscore their suitability towards satisfying necessary criteria for designing effective Ln(III) bioprobes for cellular imaging applications.

2.4. DNA binding studies

DNA is one of the most important pharmacological targets for several metal-based therapeutic drugs (cisplatin, carboplatin, oxaliplatin, Ru-drugs) [37,38]. Numerous transition metal and lanthanide complexes containing planer phenanthroline and polypyridyl ligands were utilized in DNA recognition, charge-transfer agents to nucleic acid, and serum proteins, phototherapeutic agents [20,21,39,40]. The Ln(III) complexes **1**–**5** containing dtntp ligand with two pendant planer phenyl-terpyridine antennae have allowed us to study their binding interaction with duplex DNA. Upon gradual addition of CT-DNA to the dtntp ligand and [Ln(dtntp)(H_2O)] complexes **1**–**5** results in a hypochromic shift in absorption spectra due to binding between Ln (III) complexes and the base pairs of DNA (Fig. 6a and Figs. S15-S18). The intrinsic equilibrium binding constant (K_b) for the complexes **1**–**5** were calculated are $K_b \approx 10^4$ M^{-1} and reported in Table 2 [24]. These results suggesting their moderate binding propensity with CT-DNA possibly via partial intercalation binding mode or π-π interaction through two pendant planar phenyl-terpyridine antennae moieties of dtntp with DNA base pairs [41].

Ethidium bromide (EthB), a planer cationic fluorescent dye, acts as an effective spectral probe to determine the relative binding affinity of the complexes to CT-DNA. The apparent binding constant (Kapp) of the complexes 1–5 to CT-DNA was monitored by successive changes observed in the emission band of EthB bound DNA [42]. The emission intensity of the EthB was significantly quenched upon titration with complexes ensuring the displacement of ethidium bromide (EthB) and possible partial intercalation with DNA (Fig. 6b and Figs. S19-S22). The calculated K_{app} values are (K_{app}) ~ 10^6 M^{-1} (Table 2), which suggests complexes have an efficient binding affinity with CT-DNA. The higher values of K_b and K_{app} of the complexes **1**–**5** reveals significant binding affinity to CT-DNA, possibly through partial intercalation with planar Ph-tpy moieties.

Table 1
Photophysical properties of the complexes **1**–**5.**

Complex	λ_{ex}[a](nm)/(ε/M^{-1} cm^{-1})	τH_2O[b](ms)	τD_2O[c](ms)	q[d]	$\phi_{overall}$[e](H_2O)	$\phi^f_{overall}$(D_2O)
1	284(61780)	0.45	1.08	1.2	0.231	0.378
2	284(60900)	0.65	0.80	1.1	0.178	0.297
4	284(64400)	0.27	0.39	–	0.078	0.128
5	284(63600)	0.20	0.29	–	0.048	0.086

[a] UV/visible absorption spectra.
[b, c] Luminescence lifetimes (τ) in H_2O and D_2O.
[d] Hydration number (q) calculated using modified Horrocks' equation ignoring any alternative deactivation pathways.
[e, f] Overall quantum yield ($\phi_{overall}$) of the Ln(III) complexes in H_2O and D_2O (contains 1% DMF). The experimental errors τ,±10%; q, ±10%; $\phi_{Overall}$,±10%.

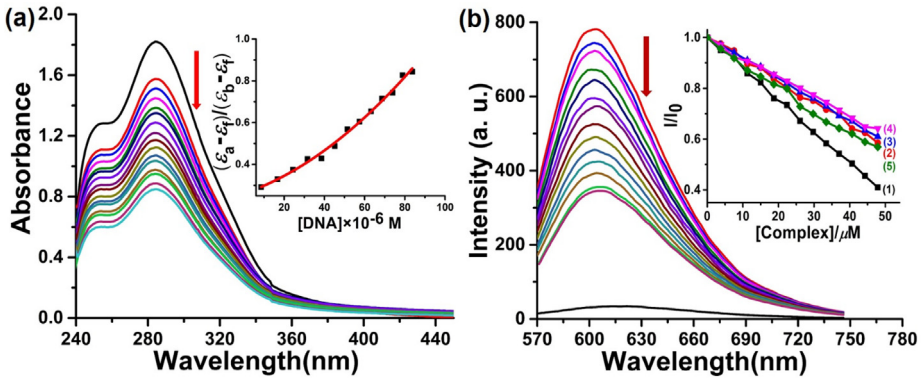

Fig. 6. (a) UV–vis spectral traces of [Eu(dtntp)(H_2O)] (**1**, 34 μM) in 5 mM Tris-buffer (pH 7.2) with increasing concentration of CT-DNA at 298 K. The inset shows $\Delta\varepsilon_{af}/\Delta\varepsilon_{bf}$ vs. [CT-DNA] plot for complex **1**. (b) Emission spectral traces of EthB bound CT-DNA with increasing amount of **1** in 5 mM Tris-buffer (pH 7.2) at 298 K, λ_{ex} = 546 nm, λ_{em} = 603 nm, [CT-DNA] = 313 μM, [EthB] = 12 μM. The inset shows plots of fluorescence intensity I/I_0 vs. [complex] for **1**–**5**.

Table 2
Binding interaction parameters for the complexes **1**–**5** with biomolecules.

	DNA		BSA			HSA		
	$K_b \times 10^4$ [M^{-1}][a]	$K_{app} \times 10^6$ [M^{-1}][b]	$K_{BSA} \times 10^5$ [M^{-1}][c]	$k_q \times 10^{13}$ [M^{-1}][d]	$K \times 10^5$ [M^{-1}][e]	$K_{HSA} \times 10^4$ [M^{-1}][c]	$k_q \times 10^{12}$ [M^{-1}]	$K \times 10^3$ [M^{-1}]
1	1.29(±0.03)	2.95	3.74(±0.02)	3.74	5.27	1.84(±0.01)	2.84	6.44
2	2.61 ± 0.02)	2.05	4.57(±0.03)	4.57	1.52	3.02(±0.04)	3.02	3.14
3	1.25(±0.04)	2.15	–	–	–	–	–	–
4	2.85(±0.03)	1.93	3.40(±0.02)	3.40	1.96	6.57(±0.12)	6.57	8.81
5	1.53(±0.02)	2.18	5.39(±0.04)	5.39	3.37	4.53(±0.02)	4.53	1.86

[a] K_b, equilibrium DNA binding constant.
[b] K_{app}, apparent DNA binding constant. For dtntp ligand: $K_b = 3.33(\pm0.03) \times 10^4$ M^{-1} and $K_{app} = 2.03(\pm0.04) \times 10^6$ M^{-1}.
[c] $K_{BSA/HSA}$, Stern-Volmer quenching constant for BSA and HSA fluorescence.
[d] k_q, quenching rate constant.
[e] K, binding constant with BSA and HSA. Number of binding sites (n) are 1.49 (**1**), 1.03 (**2**), 1.47 (**4**) and 0.92 (**5**) for BSA and 0.42 (**1**), 0.55 (**2**), 0.80 (**4**) and 0.66 (**5**) for HSA respectively.

2.5. Serum protein binding studies

Serum albumin is the most abundant blood protein, constitutes ~55% of total blood plasma. Serum protein has been the most extensively studied proteins and plays a vital role in drug transport and metabolism [43,44]. Structurally homologous bovine serum albumin (BSA) and human serum albumin (HSA) were used to study the binding interaction with present Ln(III) complexes. The intrinsic tryptophan and tyrosine residues in serum proteins are responsible for the fluorescence properties in BSA and HSA. The binding affinity of the Ln(III) complexes **1**–**5** with BSA and HSA were investigated using characteristic tryptophan emission quenching of BSA (Trp 135 and Trp 214) and HSA (Trp 214) in the presence of complexes **1**–**5**. The gradual increase of concentration of the complexes **1**–**5** results in significant quenching of emission intensity of BSA and HSA at λ = 345 nm (Fig. 7a-b and Figs. S23-S33). The changes observed in spectral intensity and shift in emission wavelengths upon binding with complexes attributed to various changes in the secondary structure of the proteins, substrate binding, or structural changes of proteins [44].

The Stern-Volmer equation has been utilized and calculated the Stern-Volmer quenching constant K_{BSA} and K_{HSA} for complexes **1**–**5** are in the range of $K_{BSA} \sim 10^5$ M^{-1} and $K_{HSA} \sim 10^4$ M^{-1} reported in Table 2 [45]. The values of binding constant (K), the number of the binding site (n) and quenching rate constant (k_q) for complexes to BSA and HSA were determined by using Scatchard equation: $\log (I_0 - I)/I = \log K + n \log[Q]$ (Fig. S26 and Fig. S33). The higher values of K_{BSA} and K_{HSA} suggest a significant binding affinity of the complexes to serum proteins, which may facilitate the transporting of such Ln(III) bioprobes to the pathological site [44d].

Synchronous emission spectroscopy study can provide critical information about the molecular microenvironment in the vicinity of fluorophores (Tyr or Trp residues) in the HSA protein [46]. In synchronous fluorescence spectra, tryptophan residues give typical emission at $\Delta\lambda$ = 60 nm and tyrosine residues give characteristic emission at $\Delta\lambda$ = 15 nm. Synchronous emission spectra of HSA were monitored with the gradual addition of increasing concentration of complexes **1**–**5** both at $\Delta\lambda$ = 15 nm and $\Delta\lambda$ = 60 nm (Fig. 7 c-d). The synchronous emission of HSA ($\Delta\lambda$ = 15 nm) with varying complex concentration results in decrease in emission intensity at 284 nm with a minor shift in the band position, indicating the effect of complexes depends less likely upon the microenvironment of the tyrosine residues in HSA. However, synchronous emission of HSA at $\Delta\lambda$ = 60 nm with the addition of **1**–**5** leads to a much-pronounced quenching of emission intensity at 280 nm with minor red-shift of peak maxima. We also observed an isosbestic point at 295 nm and a concomitant formation of a new band at 315 nm. The significant changes in synchronous fluorescence intensity indicates the altered polarity in the protein microenvironment [60].

2.6. Cellular imaging studies

The cellular uptake and distribution of the [Eu/Tb(dtntp)(H_2O)] (**1**, **2**) complexes were studied by confocal fluorescence microscopy via examining the red and green emission originating from Eu(III) and Tb(III) ions. The cytotoxicity of dtntp ligand and complexes **1, 2** were assessed using well-known MTT assay in various cancer cells (HeLa, MCF-7, and H460) are depicted in Figs. S34-S35. The IC_{50} values for **1** and **2** were reported in Table S4 and found to be mod-

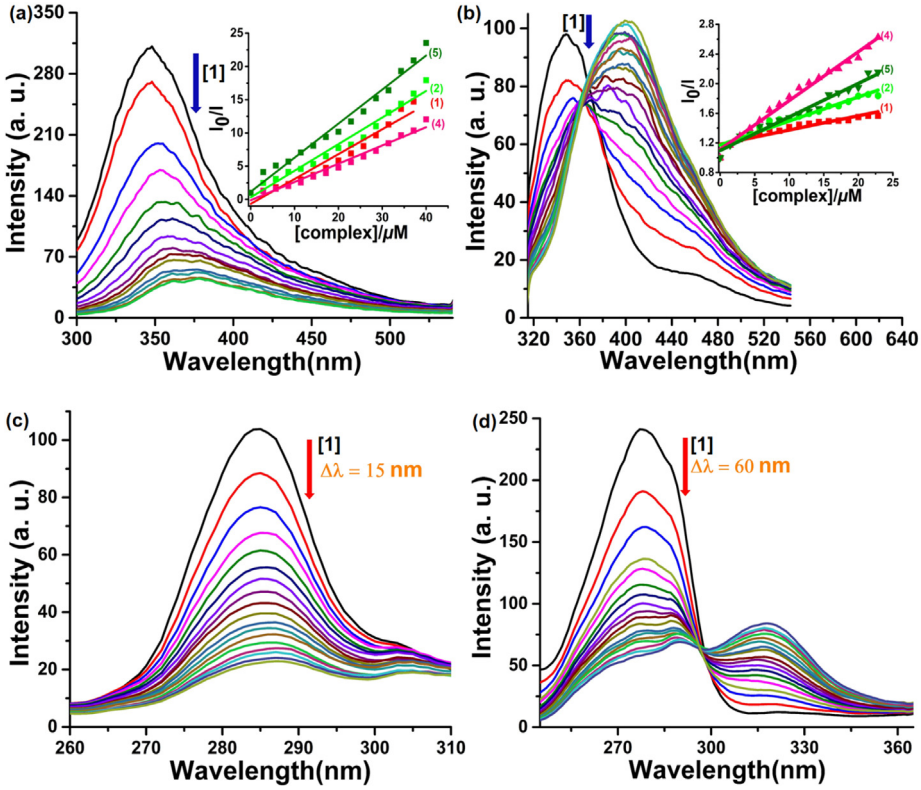

Fig. 7. (a) The effect of the addition of complex **1** on the emission spectral quenching of BSA in 5 mM Tris-buffer (pH 7.2) at 298 K. Inset: Stern–Volmer plots of the fluorescence titrations of complexes **1**–**2** and **4**–**5** with BSA. (b) Fluorescence spectral quenching of the HSA emission with the addition of an increasing amount of complex **1.** Inset: Stern–Volmer plots of **1**–**2** and **4**–**5**. λ_{ex} = 295 nm, λ_{em} = 345 nm, [BSA] = 5 μM, [HSA] = 2 μM. (c) Uncorrected synchronous fluorescence spectra of HSA protein (2 μM), in the presence of an increasing concentration of complex **1** with ex. and em. wavelength difference of $\Delta\lambda$ = 15 nm, and (d) $\Delta\lambda$ = 60 nm.

erately cytotoxic in the dark and remain significantly viable within the concentration ranges (20 μM) used for cellular imaging studies. The cellular imaging studies of the Eu(III) and Tb(III) complexes were carried out in HeLa, MCF-7, and H460 cancer cells to probe the potential uses of these luminescent Ln(III) complexes as luminescent cellular stains. The cancer cells were incubated with the solution of Eu(III) (**1**) and Tb(III) (**2**) (20 μM) complexes in DMEM for 4 h, and the nucleus was stained with Hoechst 33258 dye to determine the subcellular localization of the compounds. The fluorescence cell images of the cancer cells were captured with an excitation wavelength (λ_{ex}) of 405 nm for Eu(III) and 488 nm for the Tb (III) are shown in (Figs. 8-10 and Figs. S36-37) respectively. The cellular internalization of these Ln(III) probes was evaluated from their characteristic intense red and green emission from the excited states ($^5D_0$) of Eu(III) and ($^5D_4$) of Tb(III) respectively using multiphoton confocal laser scanning fluorescence microscopy (MCLSFM).

Confocal fluorescence images of both the complexes are confirming their significant uptake within the cells (panel-I in Figs. 8 and 9). These Ln(III) bioprobes seem most likely accumulate into the cytoplasm and nucleus. The results demonstrate that tested complexes possibly permeate through the cytoplasm, then traverse through the nuclear membrane, and ultimately enter the nuclei. Acquired confocal images of HeLa, MCF-7, and H460 cells are showing bright red, and green spots within the nuclei assigned with arrows (Fig. 10) were suggesting their sufficient localization inside the nuclei or specifically in protein-rich nucleoli [47–48,11,20].

The thermodynamically stable Eu(III)/Tb(III) complexes with longer τ and Φ values have elegantly reduced the autofluorescence and scattering from the background. The luminescence originated from the Eu(III)/Tb(III) bioprobes were stable and consistent throughout experiments suggesting their photostability and resistance towards possible photobleaching. These desirable features were essential for their utility as potential cellular imaging agents. The pendant terpyridine moieties in these complexes could be potentially exploited for their metal-binding capability or rich electronic effects.

2.7. Photocytotoxicity

Photo-responsive therapeutic agents play a critical role in cancer chemotherapy. Metal complexes are gaining increasing interest as photosensitizers in PDT and photo-activated chemotherapy (PACT) [49]. A Ru(II)-based photosensitizer (TLD1433) recently entered in clinical trials [49a]. The Ln(III) complexes with a wide window of excited-state energy levels (Vis-NIR), upconversion ability, and high degree of modularity in their design have excellent potential in photochemotherapy. The photocytotoxicity of complexes **1** and **2** were examined in the HeLa cells upon photoirradiation at 365 nm (6 W) for 1 h from the MTT assay (Fig. 11). The IC_{50} values for complexes **1** and **2** are 32.5 ± 0.8 μM and 28.6 ± 1.0 μM respectively and were found to be significantly toxic than in the dark makes them suitable for potential photo-responsive therapeutic agents [20,49b–c]. The complexes remain moderately less toxic in the dark as evidenced by cell viability assay in the dark (Figs. S34-S35) and cell imaging studies. Thus, these complexes can serve the dual purpose as a cellular imaging tool and phototherapeutic agents or light-responsive theranostic probes.

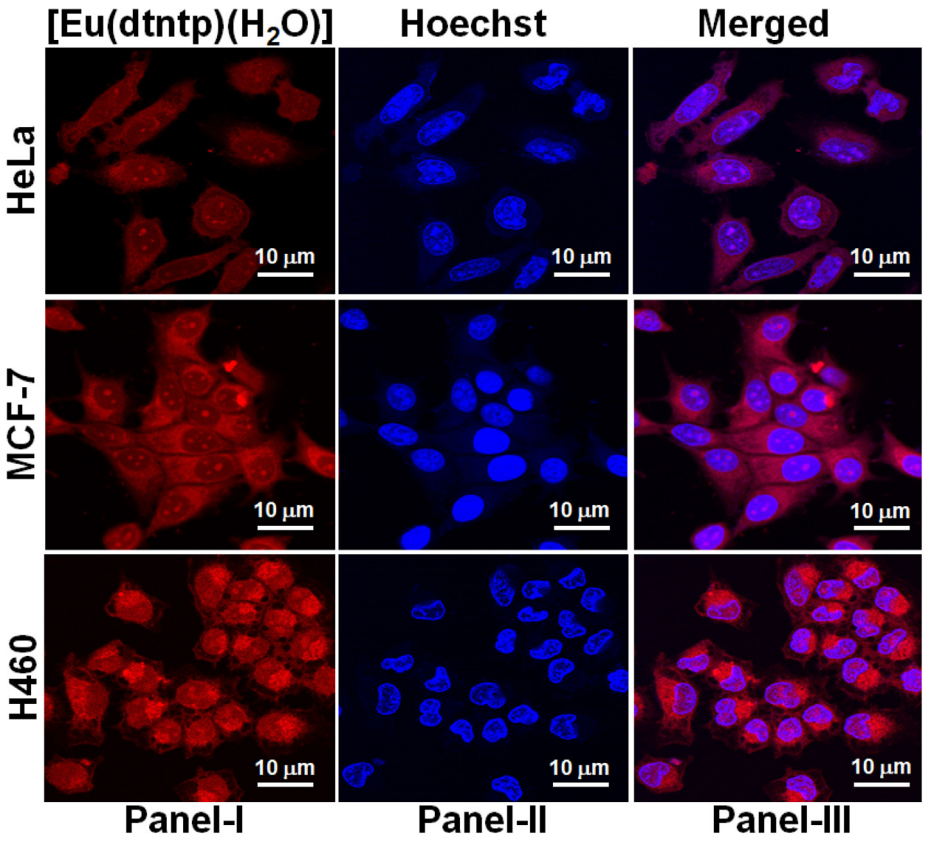

Fig. 8. MCLSFM images of the HeLa, MCF-7, H460 cells incubated with complex **1** at 20 μM for 4 h and nucleus staining Hoechst 33258 dye (5 μgmL^{-1}) showing the intracellular distribution profile of the Eu(III) complex (**1**). Panel-I: Red emission from Eu(III); Panel-II: blue emission from nucleus staining Hoechst 33258 dye; panel III: merged images showing subcellular (nuclear and cytosolic) localization of the complex; Scale bar = 10 μm and λ_{ex} = 405 nm.

3. Conclusions

We strategically designed a DTPA-bisamide derivative of eight coordinate dtntp chelator containing two phenyl-terpyridine (Ph-tpy) pendant antenna moieties to sensitize the Ln(III) ions. The ligand yields a series of structurally identical thermodynamically stable lanthanide complexes: [Ln(dtntp)(H_2O)] [Ln(III) = Eu, Tb, Gd, Sm, Dy (**1**–**5**)]. The modular design principle satisfies the dual functional prerequisites as cell imaging and photocytotoxic agents. The solid-state structure of the [Eu(dtntp)(DMF)] shows discrete nine-coordinated {EuN_3O_6} cores with distorted tricapped-trigonal prism (TTP) coordination geometry around the Eu(III). Photophysical studies reveal triplet state of dtntp and the Ln(III) emissive excited states are having suitable energy gap that allows efficient energy transfer from the dtntp pendant antenna to the Ln(III). This results in desirable optical properties and photostability of [Eu/Tb(dtntp)(H_2O)] complexes required for cellular imaging. The complexes **1**–**5** showed significant CT-DNA binding propensity possibly through partial intercalation *via* planer ph-tpy moieties of dtntp and DNA base pairs. The complexes **1**–**5** revealed efficient binding to serum proteins possibly due to various molecular interactions. The cellular imaging studies of Eu and Tb-complexes in different cancer cells reveals their cytosolic and nuclear localization ensures their potential use as cellular imaging agents. The Eu(III) and Tb(III) complexes showed enhanced photocytotoxicity in HeLa cells at 365 nm for their therapeutic utility. Thus, collectively these results are promising and offer an improved modular strategy for the development of multimodal Ln(III) bioprobes for light-responsive theranostic application.

4. Experimental section

4.1. Material and methods

Ln(III) salts ($Eu(CF_3SO_3)_3$ (98%), $Tb(CF_3SO_3)_3$ (97%), $Gd(NO_3)_3$-$\cdot 6H_2O$ (99.9%), $Dy(NO_3)_3$·hydrate (99.9%), $SmCl_3 \cdot 6H_2O$ (99.98%)), Diethylenetriaminepentaacetic dianhydride from Sigma-Aldrich. All other reagents and solvents were purchased from commercial sources (Sigma-Aldrich, Alfa Aesar, Fisher Scientific) and used without further purification unless otherwise mentioned. 4′-(4-aminophenyl)-2,2′:6′,2″-terpyridine was synthesized according to the literature procedure [24b,50]. HeLa, MCF-7 and H460 cancer cells were obtained from National Center for Cell Sciences, Pune, India. FT-IR spectral data were recorded using KBr pellets on a Perkin-Elmer model 1320 FT-IR spectrometer. Electrospray Ionization Mass spectrometry (ESI-MS) spectra were acquired by using Waters Q-TOF Premier mass spectrometer.

4.2. Photophysical measurements

Absorption spectral data were recorded at 298 K using Perkin-Elmer Lambda 25 spectrophotometer. All the steady state fluorescence emission and time-delayed luminescence spectral data were monitored on Agilent Cary Eclipse fluorescence spectrophotometer at 298 K. Excitation spectra of complexes **1**–**5** in aqueous-DMF at 298 K were measured by fixing their corresponding major Ln(III) ions emission wavelength (λ_{em} = 615 nm (**1**), λ_{em} = 545 nm (**2**), λ_{em} = 410 nm (**3**), λ_{em} = 598 nm (**4**), λ_{em} = 570 nm (**5**) respectively. Luminescence lifetime (τ) measurements were recorded under ambient conditions in H_2O and D_2O (contains 1% DMF) using a

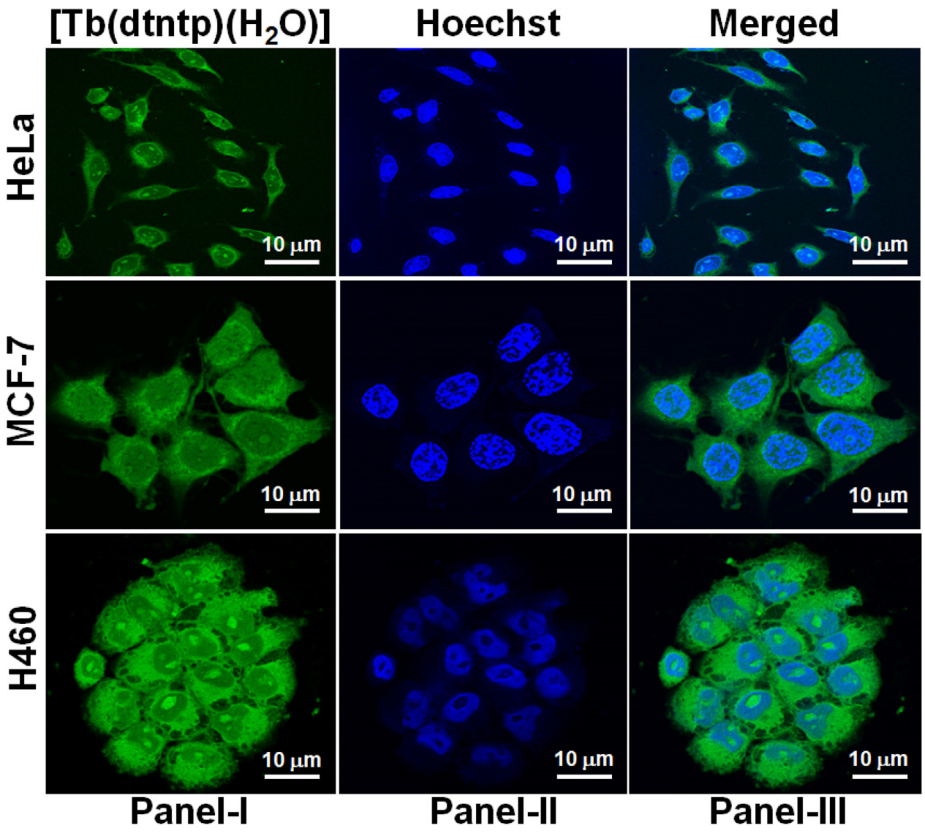

Fig. 9. MCLSFM images of the HeLa, MCF-7, H460 cells incubated with complex **2** at 20 μM for 4 h and nucleus staining Hoechst 33258 dye (5 μgmL^{-1}) showing the intracellular distribution profile from Tb(III) complex (**2**). Panel-I: Green emission from Tb(III); panel-II: blue emission from nucleus staining Hoechst 33258 dye; panel III: merged images showing subcellular (nuclear and cytosolic) localization of the complex; Scale bar = 10 μm and λ_{ex} = 488 nm.

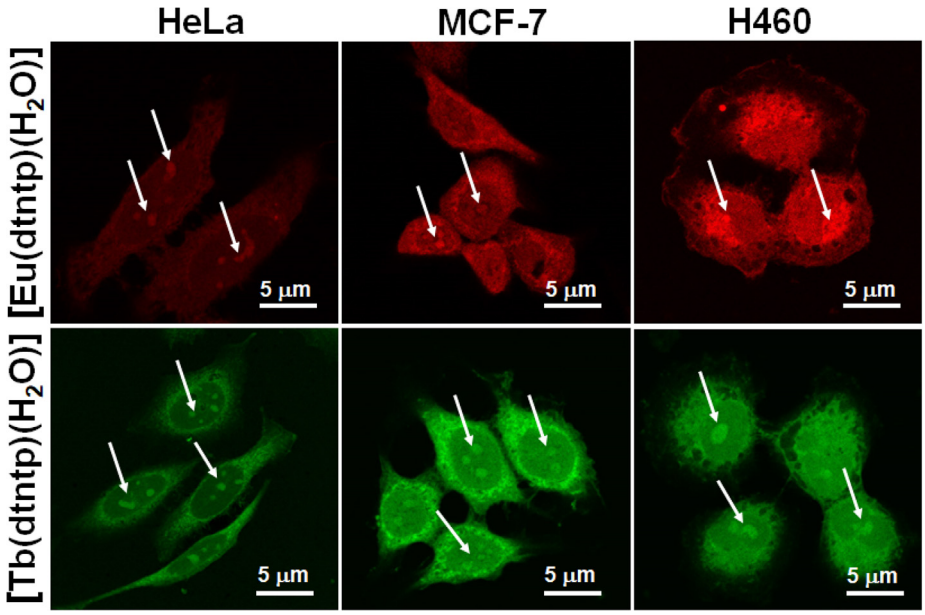

Fig. 10. MCLSFM imaging study of the complexes **1** (upper row), and **2** (lower row) in HeLa, MCF-7, and H460 cancer cells showing cellular behavior of Eu(III) and Tb(III) respectively. Bright red and green spots are shown with arrows distinguishing localization of **1** and **2** into cell nuclei. Scale bar = 5 μm.

pulsed Xenon lamp at excitation wavelength (λ_{ex}) of 284 nm, and emission wavelength (λ_{em}) at 615 nm and 545 nm for Eu(III) and Tb(III) complexes (**1, 2**) and 598 nm and 570 nm for Sm(III) and Dy(III) complexes (**4, 5**) respectively with a delay/gate time of 0.1 ms. Emission decay curves were fitted by a single exponential fitting using the non-linear least square method. Lifetime data for complexes **1**–**5** in H_2O and D_2O contains 1% DMF was shown in Figs. S13-S14 and Table 1. In complexes **1** and **2,** the excited-state lifetime measurements in H_2O and D_2O allowed us to determine the number of water molecules (q) directly coordinated to

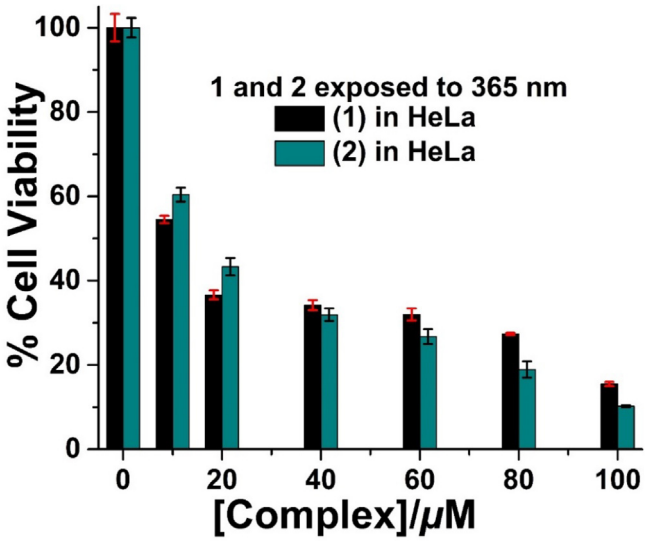

Fig. 11. Cell viability plots of HeLa cells treated and incubated with complexes **1** and **2** for 4 h in the dark followed by irradiated to UV-A light at 365 nm (6 W) for 1 h showing the photocytotoxicity activity.

the respective Ln(III) using the following modified Horrocks' equations for Eu(III) (**1**) and Tb(III) (**2**), [34].

$$q_{Eu} = 1.2\left(\frac{1}{\tau_{H_2O}} - \frac{1}{\tau_{D_2O}} - 0.25\right), q_{Tb} = 5.0\left(\frac{1}{\tau_{H_2O}} - \frac{1}{\tau_{D_2O}} - 0.06\right)$$

The overall emission quantum yields (Φ) of the complexes (**1**–**2** and **4**–**5**) were measured at 298 K using quinine sulfate as reference using the following equation:[45]

$$\varnothing_{overall} = \varnothing_{ref}\frac{A_{ref}In^2}{AI_{ref}n_{ref}^2}$$

Where *A*, *I* and *n* denote the respective absorbance at λ_{ex}, area under the emission curve and refractive index of the solvent respectively. The ϕ_{ref} represents the reference standard quinine sulfate solution quantum yield.

4.3. Synthesis and characterization

Synthesis of Bis(4′-(4-aminophenyl)-2,2′:6′,2″-terpyridine) derivative of dtpa [dtpa(Aph-tpy)$_2$ (dtntp)]. A mixture of 4′-(4-aminophenyl)-2,2′:6′,2″-terpyridine (1.09 g, 3.36 mmol, 2 equiv) and diethylenetriaminepentaacetic acid bisanhydride (600 mg, 1.68 mmol, 1 equiv) in dry DMF (20 mL) was stirred overnight at 70 °C. Diethyl ether (100 mL) was added to the reaction mixture at 0 °C, and the desired dtntp ligand precipitate formed were then filtered and washed twice with 10 mL of Et_2O, and finally dried in vacuum over P_4O_{10} and to yields crystalline product.

dtntp: Yield ~87% (1.478 g). FT-IR (KBr, cm^{-1}): 3418 (w, br, ν_{N-H}), 3264 (w), 3051(m), 2925(m), 2850(m), 1665 (vs, $\nu_{C=O}$, CO free acid), 1601 (s, $\nu_{C=O(CONH)}$ amide I), 1584 (s, $\nu_{C=O(CONH)}$ amide II), 1521(s), 1467(s), 1441(vs), 1413(m), 1388(vs) 1318(m), 1254(s), 1227(m), 1092(vs), 1039(m), 990(m), 893(m), 837(vs), 791(vs), 660(vs), 516(m). ESI-MS (in DMF): *m*/*z* (%) calcd. For $[M+H]^+$, 1006.4000(100), 1007.4000(66), 1008.4000(23), 1009.4000(6); found, 1006.4008(100), 1007.4078(63), 1008.4085(23), 1009.3909(6). Elemental analysis: Calcd. for $C_{56}H_{51}N_{11}O_8$: 66.85; H, 5.11; N, 15.31. Found: C, 66.78; H, 5.07; N, 15.24. UV–vis (in aqueous-DMF) [λ_{max}/nm (ε/M^{-1} cm^{-1})]: 383(2040), 324(25300), 295(60600), 284(62500).

Synthesis and Characterization of [Ln(dtntp)(H$_2$O)] (Ln (III) = Eu(III), Tb(III), Gd(III), Sm(III), Dy(III)). Lanthanide(III) (Ln (III) = Eu(**1**), Tb(**2**), Gd(**3**), Sm(**4**), Dy(**5**), complexes of the dtntp were synthesized by following a generalized synthetic procedure in which a hot methanolic solution of $Eu(CF_3SO_3)_3$ (0.200 g, 0.334 mmol) and $Tb(CF_3SO_3)_3$ (0.200 g, 0.330 mmol), $Gd(NO_3)_3$·$6H_2O$, (0.200 g, 0.443 mmol), $SmCl_3·6H_2O$ (0.200 g, 0.548 mmol), $Dy(NO_3)_3$·hydrate (0.200 g, 0.574 mmol), in 10 mL of boiling methanol was added drop wise to 30 mL hot stirred methanolic solution of dtntp (0.336 g, 0.334 mmol) (**1**), and (0.332 g, 0.330 mmol) (**2**), (0.446 g, 0.443 mmol) (**3**), (0.552 g, 0.548 mmol) (**4**), (0.577 g, 0.574 mmol) (**5**), pretreated with 3 equivalents of NaOH for 30 min. The reaction mixture was refluxed for 12 h on oil bath at 70 °C under nitrogen atmosphere. The solvent was evaporated in the reduced pressure and re-dissolved in the small amount of MeOH and precipitated by the addition of Et_2O. which was then filtered and washed with 10 mL of hot MeOH, 10 mL of Et_2O, and finally dried in vacuum over P_4O_{10}. The complex **1** was dissolved in DMF/MeOH and slow evaporation with addition of Et_2O/MeCN at RT after couple of months yields a very small block shaped yellowish single crystals were obtained suitable for X-ray crystallography. The solid-state structure of complex **1** shows Eu (III) 9th coordination site is occupied by the DMF solvent due to the solvent of crystallization.

[Eu(dtntp)(H$_2$O)] (1). Yield ~84% (0.463 g). ESI-MS (in DMF): *m*/*z* (%) calcd. For $[M-H_2O+H]^+$, 1156.2958(100), 1154.2958(76), 1155.2958(50), 1157.2958(58), 1158.2958(20). Found: 1156.2974 (100), 1154.2844(74), 1155.2928(50), 1157.2986(57), 1158.3029 (21). FT-IR (KBr, cm^{-1}): 3405(w, br, $\nu_{N-H)}$, 2923(m), 2850(m), 1602(vs, νasym (CO_2^-)), 1517(s, $\nu_{C=O(CONH)}$ amide), 1469(s), 1442 (vs), 1392(vs, νasym (CO_2^-)) 1324(s), 1257(s), 1166(m), 1118(s), 1092(vs), 1032(m), 993(m), 928(m), 838(vs), 792(vs), 516(m). UV–vis (aqueous-DMF) [λ_{max}/nm (ε/M^{-1} cm^{-1})]: 284(61780), 294 (59500), 324(21800). Lifetimes (τ/ms): 0.455 (H_2O), 1.087 (D_2O); Hydration number (*q*) = 1.23 at 298 K.

[Tb(dtntp)(H$_2$O)] (2). Yield ~84% (0.328 g). ESI-MS (in DMF): *m*/*z* (%) calcd. For $[M-H_2O+H]^+$, 1162.3013(100), 1163.3013(67), 1164.3013(23), 1165.3013(8). Found. 1162.3020(100), 1163.3035 (65), 1164.3029(23), 1165.3032(6). FT-IR (KBr, cm^{-1}): 3412(w, br, $\nu_{N-H)}$, 2919(m), 2850(m), 1601(vs, νasym (CO_2^-)), 1518(s, $\nu_{C=O(CONH)}$ amide), 1470(s), 1441(vs), 1385(vs, νsym (CO_2^-)) 1321(s), 1260(s), 1185(m), 1118(s), 1097(vs), 1039(m), 993(m), 928(m), 838(vs), 792(vs), 518(m). UV–vis (aqueous-DMF) [λ_{max}/nm (ε/M^{-1} cm^{-1})]: 284(60900), 294(58800) 324(21770). Lifetimes (τ/ms): 0.654 (H_2O), 0.803 (D_2O); Hydration number (*q*) = 1.12 at 298 K.

[Gd(dtntp)(H$_2$O)] (3). Yield ~84% (0.328 g). ESI-MS (in DMF): *m*/*z* (%) calcd. For $[M-H_2O+H]^+$, 1161.2957(100), 1158.2957(40), 1159.2957(75), 1160.2957(80), 1162.2957(52), 1163.2957(70), 1164.2957(39), 1165.2975(13). Found: 1161.3004(100), 1158.2976(35), 1159.3009(69), 1160.2975(80), 1162.2990(52), 1163.3052(68), 1164.2996(38), 1165.3009(14). FT-IR (KBr, cm^{-1}): 3435(w, br, $\nu_{(N-H)}$, 2918(m), 2849(m), 1601(vs, νasym (CO_2^-)), 1517(s, $\nu_{C=O(CONH)}$ amide), 1468(s), 1440(vs), 1384(vs, νsym (CO_2^-)), 1321(s), 1259(s), 1184(m), 1118(s), 1092(vs), 1055(m), 994(m), 929(m), 837(vs), 791(vs), 513(m). UV–vis (aqueous-DMF) [λ_{max}/nm (ε/M^{-1} cm^{-1})]: 284(53800), 294(52500), 324(20950).

[Sm(dtntp)(H$_2$O)] (4). Yield ~85% (0.550 g). ESI-MS (in DMF): *m*/*z* (%) calcd. for $[M-H_2O+H]^+$, 1155.2885(100), 1150.2885(52), 1151.2885(72), 1152.2885(84), 1153.2885(67), 1154.2885(30), 1156.2885(62), 1157.2885(98), 1158.2885(56), 1159.2885(18). Found: 1155.2983(100), 1150.2997(48), 1151.2979(72), 1152.2916(79), 1153.2965(68), 1154.2937(32), 1156.3057(64), 1157.3070(96), 1158.2949(56), 1159.2423(21). FT-IR (KBr, cm^{-1}): 3435(w, br, $\nu_{N-H)}$, 2924(m), 2852(m), 1603(vs, νasym (CO_2^-)), 1518(s, $\nu_{C=O(CONH)}$ amide), 1468(s), 1441(vs), 1392(vs, νsym (CO_2^-)), 1325(s), 1263(s), 1187(m), 1118(s), 1092(vs), 1039(m), 993(m), 930(m), 837(vs), 791(vs), 517(m). UV–vis (aqueous-DMF) [λ_{max}/nm (ε/M^{-1} cm^{-1})]: 284(64400), 294(62200), 324(24500). Lifetimes (τ/ms): 0.268 (H_2O), 0.387 (D_2O).

[Dy(dtntp)(H_2O)] (5). Yield ~84% (0.576 g). ESI-MS (in DMF): *m/z* (%) calcd. For $[M-H_2O]^+$, 1166.2939(100), 1164.2939(74), 1165.2939(89), 1167.2939(50), 1168.2939(15), 1169.2939(4), found. 1166.2996(100), 1164.3040(69), 1165.3003(84), 1167.3015(50), 1168.3081(15), 1169.3069(4). FT-IR (KBr, cm^{-1}): 3430(w, br, $\nu_{N-H)}$, 2919(m), 2850(m), 1600(vs, νasym (CO_2^-)), 1516(s, $\nu_{C=O(CONH)}$ amide), 1469(s), 1441(vs), 1384(vs, νsym (CO_2^-)), 1324(s), 1260(s), 1184(m), 1116(s), 1093(vs), 1039(m), 995(m), 931(m), 837(vs), 792(vs), 517(m). UV–vis (aqueous-DMF) [λ_{max}/nm (ε/M^{-1} cm^{-1})]: 284(63600), 294(61650) 324(23800). Lifetimes (τ/ms): 0.198 (H_2O), 0.287 (D_2O).

4.4. Single-Crystal X-ray structure determination

Suitable X-ray quality crystals were mounted and all geometric and intensity data were collected on a Bruker SMART II diffractometer equipped with a graphite monochromator with Mo Kα radiation at 100(2) K. The data integration and reduction were processed with SAINT software,[51] and the data absorption corrections were made by using Bruker SADABS program [52]. The structures were solved by direct methods using the SHELXS program package and refined by the full matrix least-squares method based on F2 by using the SHELX-2017 program (Sheldrick 2017) [53]. The structures were further refined and processed with the SHELX-2017 incorporated into the Olex2 software package [54]. All non–hydrogen atoms were refined anisotropically till convergence is reached. All hydrogen atoms were placed geometrically and refined using the riding model. Some of the highly disordered solvent molecules in **1** were removed using the solvent mask command of Olex2 software [54]. Perspective views of the complex were obtained using ORTEP [55]. Selected crystallographic data and structure refinement parameters for **1** was given in Table S1. Selected bond distances and angles for all the complexes are given in Table S2. The CCDC deposition numbers for complex **1** is 1,991,342 containing supplementary crystallographic data.

4.5. DNA and serum proteins binding experiments

DNA, BSA and HSA binding studies were carried out by employing procedure reported by us previously [20]. The DNA binding experiments were carried out in 5 mM Tris-HCl-NaCl buffer (pH = 7.2) using calf thymus (CT)-DNA by absorption spectral measurement. The concentration of DNA was calculated from its known molar absorptivity at λ_{260} nm (ε_{260} = 6600 $M^{-1}cm^{-1}$) and the purity was confirmed from absorbance ratio A_{260}/A_{280} (1.8–1.9) [56]. A stock solution was prepared freshly and the intrinsic binding constant (K_b) of the **1**–**5** were obtained from the slope to intercept ratio of the following equation:

$$[DNA]/(\varepsilon_a - \varepsilon_f) = [DNA]/(\varepsilon_b - \varepsilon_f) + 1/K_b(\varepsilon_b - \varepsilon_f)$$

Where [DNA] is the concentration of DNA in the base pairs, ε_a, ε_f, and ε_b where the molar extinction coefficient of the complexes corresponding to apparent, free and fully bound to DNA [57]. The competitive DNA binding of complexes with ethidium bromide (EthB) was measured from the gradual addition of the complexes to highly fluorescent CT-DNA and EthB adduct (λ_{ex} = 546 nm and λ_{em} = 603 nm) in Tris-HCl/NaCl buffer (pH = 7.2). The apparent binding constant of complexes with CT-DNA obtained from equation: $K_{app} \times C_{50} = K_{EthB} \times$ [EthB], where, K_{app}, the apparent binding constant of the complex studied; C_{50}, the [complex] at 50% quenching of DNA-bound EthB emission intensity and K_{EthB}, the binding constant of EthB (1×10^7 M^{-1}) itself and [EthB] is the concentration of EthB (12 μM) used [58].

4.6. Protein binding experiments

The fluorescence emission quenching of tryptophan at 345 nm (λ_{ex} = 280 nm) of serum protein namely BSA/HSA in Tris-HCl/NaCl buffer (pH = 7.2) were performed to study the binding interaction of complexes. The addition of quencher (complexes **1**–**5**) to serum proteins lead to the gradual decrease of emission intensity, the quenching constant ($K_{BSA/HSA}$) and quenching rate constant (K_q) were determined from a linear fit of Stern-Volmer equation:[45]

$$I_0/I = 1 + K_{BSA/HSA}[Q]I_0/I = 1 + k_q\tau_0[Q]$$

where the terms I_0 and I are the emission intensities of serum proteins before and after the addition of complex concentration [Q] and τ_0 is the average lifetime of chromophore tryptophan residue of the protein in free from the quencher, any possible inner-filter effect was not considered. The equilibrium binding constant (K) of complexes **1**–**5** with BSA and HSA proteins and the number of binding sites available (n) per molecule of the proteins were calculated from the intercept and slope of the linear fit of the Scatchard equation: [59] $\log(I_0\text{-}I)/I = \log K + n\log[Q]$.

Synchronous fluorescence spectra of the complexes were recorded using the $\Delta\lambda$ = 60 nm and $\Delta\lambda$ = 15 nm ($\Delta\lambda$ = difference of excitation and emission wavelengths) respectively in 5 mM Tris-HCl/NaCl between the range of 230 nm and 500 nm under the similar condition of fluorescence quenching experiments.

4.7. Cellular uptake studies

HeLa, MCF-7 and H460 cancer cells were cultured in DMEM cell culture media supplemented with 10% fetal bovine serum (FBS) in 5% CO_2 at 37 °C and 99% humidified incubator. The cancer cells from the exponentially growing cultures were used for the cytotoxicity, photocytotoxicity and cellular internalization studies. The cytotoxicity and photocytotoxicity of complexes **1** and **2** were determined by MTT assay by employing the procedure described earlier [20]. Ln(III) complexes **1** and **2** (20 μM) were dissolved in the DMEM cell culture media containing 1% DMSO. The HeLa, MCF-7 and H460 cells were seeded (1×10^4 cells per well) in sterilized glass coverslip containing 24 well plates (13 mm, 0.2% gelatin-coated) for 10 h. Complexes **1** and **2** were added for incubation of 4 h at 37 °C in a 5% CO_2-humidified incubator. Then, treated cells were washed thrice with 1X PBS buffer in an interval of 5 min to remove the debris and fixed with 4% formaldehyde solution for 20 min and subsequent removal of excess formaldehyde by 1X PBS buffer. Subsequently, cell nuclei were stained with Hoechst 33258 dye for about 15 min, and the excess stain was removed by washing thrice with 1X PBS buffer. Coverslips were then mounted on slides coated with buffered mounting medium to prevent fading and drying. The slides were observed and fluorescence images of the Ln(III) complexes were acquired with Carl Zeiss (LSM780NLO) multiphoton confocal laser scanning microscopy (MCLSM) with the inverted motorized stand (AxioObserver, Zeiss) at 40X magnification. The emission in cellular images were collected by excitation wavelength (λ_{ex}) for Eu(III) 405 nm and for Tb(III) 488 nm respectively. To avoid the scattering from samples and emission from the staining dye we were applied appropriate bandpass filters for blue (blue ch1: 371–486 nm), red (red ch2: 563–739 nm) and green (green ch1: 490–544 nm) emission from Hoechst 33258, and Eu (III) and Tb(III) respectively.

CRediT authorship contribution statement

Srikanth Dasari: Conceptualization, Methodology, Data curation, Validation, Writing - original draft. **Swati Singh:** Data curation. **Zafar Abbas:** Data curation, Investigation. **Sri Sivakumar:**

Data curation, Investigation. **Ashis K. Patra:** Supervision, Conceptualization, Writing - review & editing, Funding acquisition.

Declaration of Competing Interest

The authors declare that they have no known competing financial and personal relationships that could influence the work reported herein.

Acknowledgments

We thank Science and Engineering Research Board (SERB), Government of India (Grant No. EMR/ 2016/000521) for financial support. S.D thanks MHRD and ZA to U.G.C. for research fellowships. Thanks to Priyaranjan Kumar for fruitful discussions and Sharad Sachan for his help and discussion in the solving crystal structure.

Appendix A. Supplementary material

Supplementary Information (SI) available: Spectral characterization, additional crystallographic figures, photophysical properties, binding interaction with biological targets, cell culture, cytotoxicity, photocytotoxicity and cell imaging figures (PDF). For SI and crystallographic data in CIF or other electronic format see https://doi.org/10.1016/j.saa.2021.119709.

References

[1] (a) P. Caravan, J.J. Ellison, T.J. McMurry, R.B. Lauffer, Chem. Rev. 99 (1999) 2293–2352;
(b) P. Caravan, Chem. Soc. Rev. 35 (2006) 512–523;
(b) E.J. Werner, A. Datta, C.J. Jocher, K.N. Raymond, Angew. Chem. Int. Ed. 47 (2008) 8568–8580.
[2] (a) J.-C.G. Bünzli, Chem. Rev. 110 (2010) 2729–2755;
(b) J.-C.G. Bünzli, S.V. Eliseeva, Chem. Sci. 4 (2013) 1939–1949;
(d) J.-C.G. Bünzli, Coord. Chem. Rev. 293–294 (2015) 19–47.
[3] (a) C.P. Montgomery, B.S. Murray, E.J. New, R. Pal, D. Parker, Acc. Chem. Res. 42 (2009) 925–937;
(b) E.J. New, D. Parker, D.G. Smith, J.W. Walton, Curr. Opin. Chem. Biol. 14 (2010) 238–246.
[4] (a) M.C. Heffern, L.M. Matosziuk, T.J. Meade, Chem. Rev. 114 (2014) 4496–4539;
(b) T. Gunnlaugsson, J.P. Leonard, Chem. Commun. (2005) 3114–3131;
(c) A.J. Amoroso, S.J.A. Pope, Chem. Soc. Rev. 44 (2015) 4723–4742.
[5] (a) E.G. Moore, A.P.S. Samuel, K.N. Raymond, Acc. Chem. Res. 42 (2009) 542–552;
(b) M. Sy, A. Nonat, N. Hildebrandt, L.J. Charbonnière, Chem. Commun. 52 (2016) 5080–5095.
[6] R.D. Teo, J. Termini, H.B. Gray, J. Med. Chem. 59 (2016) 6012–6024.
[7] V.C. Pierre, M.J. Allen, P. Caravan, J. Biol. Inorg. Chem. 19 (2014) 127–131.
[8] (a) F.G. Shellock, E. Kanal, J. Magn. Reson. Imaging 10 (1999) 477–484;
(b) M.E. Bartolini, J. Pekar, D.R. Chettle, F. McNeill, A. Scott, J. Sykes, F.S. Prato, G.R. Moran, Magn. Reson. Imaging 21 (2003) 541–544;
(c) M. Ceulemans, K. Nuyts, W.M. De Borggraeve, T.N. Parac-Vogt, Inorganics 3 (2015) 516–533.
[9] E. Debroye, T.N. Parac-Vogt, Chem. Soc. Rev. 43 (2014) 8178–8192.
[10] (a) A. Louie, Chem. Rev. 110 (2010) 3146–3195;
(b) L. Frullano, T.J. Meade, J. Biol. Inorg. Chem. 12 (2007) 939–949.
[11] (a) S.J. Butler, L. Lamarque, R. Pal, D. Parker, Chem. Sci. 5 (2014) 1750–1756;
(b) S.J. Butler, M. Delbianco, L. Lamarque, B.K. Mc Mahon, E.R. Neil, R. Pal, D. Parker, J.W. Walton, J.M. Zwier, Dalton Trans. 44 (2015) 4791–4803.
[12] (a) A. Thibon, V.C. Pierre, Anal. Bioanal. Chem. 394 (2009) 107–120.
[13] (a) S. Faulkner, S.J.A. Pope, B.P. Burton-Pye, Appl. Spectrosc. Rev. 40 (2005) 1–31.
[14] (a) M. Delbianco, V. Sadovnikova, E. Bourrier, G. Mathis, L. Lamarque, J.M. Zwier, D. Parker, Angew. Chem. Int. Ed. 53 (2014) 10718–10722;
(b) E.J. New, A. Congreve, D. Parker, Chem. Sci. 1 (2010) 111–118;
(b) S. Shuvaev, M. Starck, D. Parker, Chem. Eur. J. 23 (2017) 9974–9989.
[15] (a) S.S. Kelkar, T.M. Reineke, Bioconjugate Chem. 22 (2011) 1879–1903;
(b) P. Rai, S. Mallidi, X. Zheng, R. Rahmanzadeh, Y. Mir, S. Elrington, A. Khurshid, T. Hasan, Adv. Drug Deliv. Rev. 62 (2010) 1094–1124;
(c) S. Wilhelm, A.J. Tavares, Q. Dai, S. Ohta, J. Audet, H.F. Dvorak, W.C.W. Chan, Nat. Rev. Mater. (2016) 16014.
[16] (a) J.L. Sessler, R.A. Miller, Biochem. Pharmacol. 59 (2000) 733–739;
(b) G. Thiabaud, R. McCall, G. He, J.F. Arambula, Z.H. Siddik, J.L. Sessler, Angew. Chem. Int. Ed. 55 (2016) 12626–12631;
(c) Z. Zhu, X. Wang, T. Li, S. Aime, P.J. Sadler, Z. Guo, Angew. Chem. Int. Ed. 53 (2014) 13225–13228.
[17] (a) T. Zhang, C.-F. Chan, R. Lan, H. Li, N.-K. Mak, W.-K. Wong, K.-L. Wong, Chem. Commun. 49 (2013) 7252–7254;
(b) T. Zhang, R. Lan, C.-F. Chan, G.-L. Law, W.-K. Wong, K.-L. Wong, Proc. Natl. Acad. Sci. U. S. A. 111 (2014) E5492–E5497;
(c) H. Li, R. Lan, C.-F. Chan, L. Jiang, L. Dai, D.W.J.K. Wong, M.H.-W. Lam, K.-L. Wong, Chem. Commun. 51 (2015) 14022–14025;
(d) H. Li, C. Xie, R. Lan, S. Zha, C.-F. Chan, W.-Y. Wong, K.-L. Ho, B.D. Chan, Y. Luo, J.-X. Zhang, G.-L. Law, W.C.S. Tai, J.-C.G. Bünzli, K.-L. Wong, J. Med. Chem. 60 (2017) 8923–8932.
[18] (a) P. Zhang, W. Steelant, M. Kumar, M. Scholfield, J. Am. Chem. Soc. 129 (2007) 4526–4527;
(b) S.S. Lucky, N.M. Idris, Z. Li, K. Huang, K.C. Soo, Y. Zhang, ACS Nano 9 (2015) 191–205;
(c) N.M. Idris, M.K. Gnanasammandhan, J. Zhang, P.C. Ho, R. Mahendran, Y. Zhang, Nat. Med. 18 (2012) 1580–1585.
[19] (a) Z. Liang, T.-H. Tsoi, C.-F. Chan, L. Dai, Y. Wu, G. Du, L. Zhu, C.-S. Lee, W.-T. Wong, G.-L. Law, K.-L. Wong, Chem. Sci. 7 (2016) 2151–2156;
(b) H. Li, R. Lan, C.-F. Chan, G. Bao, C. Xie, P.-H. Chu, W.C.S. Tai, S. Zha, J.X. Zhang, K.-L. Wong, Chem. Commun. 53 (2017) 7084–7087.
[20] (a) S. Dasari, S. Singh, S. Sivakumar, A.K. Patra, Chem. Eur. J. 22 (2016) 17387–17396;
(b) S. Dasari, S. Singh, P. Kumar, S. Sivakumar, A.K. Patra, Eur. J. Med. Chem. 163 (2019) 546–559;
(c) S. Dasari, A.K. Maparu, Z. Abbas, P. Kumar, H. Birla, S. Sivakumar, A.K. Patra, Eur. J. Inorg. Chem. 31 (2020) 2998–3009;
(d) Z. Abbas, P. Singh, S. Dasari, S. Sivakumar, A.K. Patra, New J. Chem. 44 (2020) 15685–15697.
[21] (a) A. Chandra, K. Singh, S. Singh, S. Sivakumar, A.K. Patra, Dalton Trans. 45 (2016) 494–497;
(b) K. Singh, S. Singh, P. Srivastava, S. Sivakumar, A.K. Patra, Chem. Commun. 53 (2017) 6144–6147.
[22] (a) D.J. Lewis, F. Moretta, T. Hollooway, Z. Pikramenou, Dalton Trans. 41 (2012) 13138–13146;
(b) E. Debroye, S.V. Eliseeva, S. Laurent, L.V. Elst, S. Petoud, R.N. Muller, T.N. Parac-Vogt, Eur. J. Inorg. Chem. (2013) 2629–2639;
(c) A. Sebastian, M.K. Mahato, E. Prasad, Soft Matter 15 (2019) 3407–3417.
[23] (a) G. Dehaen, P. Verwilst, S.V. Eliseeva, S. Laurent, L.V. Elst, R.N. Muller, W.M. De Borggraeve, K. Binnemans, T.N. Parac-Vogt, Inorg. Chem. 50 (2011) 10005–10014;
(b) G. Dehaen, S.V. Eliseeva, P. Verwilst, S. Laurent, L.V. Elst, R.N. Muller, W.D. Borggraeve, K. Binnemans, T.N. Parac-Vogt, Inorg. Chem. 51 (2012) 8775–8783;
(c) K. Kimpe, T.N. Parac-Vogt, S. Laurent, C. Piérart, L. Vander Elst, R.N. Muller, K. Binnemans, Eur. J. Inorg. Chem. (2003) 3021–3027.
[24] (a) K. Singh, S. Banerjee, A.K. Patra, RSC Adv. 5 (2015) 107503–107513;
(b) S. Ghosh, Z. Abbas, S. Dasari, A.K. Patra, J. Lumin. 187 (2017) 46–52;
(c) K. Singh, A. Goenka, S. Ganesh, Ashis K. Patra, Eur. J. Inorg. Chem. (2018) 3942–3951.
[25] F. Wan, L. Wang, W. Xu, C. Li, Y. Li, C. Zhang, L. Jiang, Polyhedron, 145 (2018) 141–146; (b) FU-X. Wan, T-K. Zhang, Y. Li, C.-C. Li, L. Jiang, J. Chil. Chem. Soc. 61 (2016) 2.
[26] (a) D. Parker, K. Pulukkody, F.C. Smith, A. Batsanov, J.A.K. Howard, J. Chem. Soc. Dalton Trans. (1994) 689–693.
[27] (a) D. Parker, R.S. Dickins, H. Puschmann, C. Crossl, J.A.K. Howard, Chem. Rev. 102 (2002) 1977–2010.
[28] (a) M.S. Konings, W.C. Dow, D.B. Love, K.N. Reymond, S.C. Quay, S.M. Rocklage, Inorg. Chem. 29 (1990) 1488–1491;
(b) S.J. Franklin, K.N. Raymond, Inorg. Chem. 33 (1994) 5794–5804.
[29] (a) S. Aime, F. Benetollo, G. Bombieri, S. Colla, M. Fasano, S. Paoletti, Inorg. Chim. Acta 254 (1997) 63–70;
(b) Y.-M. Wang, Y.-J. Wang, R.-S. Sheu, G.-C. Liu, W.-C. Lin, J.-H. Liao, Polyhedron 18 (1999) 1147–1152;
(c) P. Hermann, J. Kotek, V. Kubíček, I. Lukeš, Dalton Trans. (2008) 3027–3047.
[30] (a) M. Latva, H. Takalo, V.M. Mukkala, C. Matachescu, J.C. Rodriguez Ubis, J. Kanakare, J. Lumin. 75 (1997) 149–169;
(b) S.B. Meshkova, Z.M. Topilova, D.V. Bolshoy, S.V. Beltyukova, Acta. Phy. Pol. A. 95 (1999) 983–990;
(c) R. Devi, R. Boddula, J. Tagare, A.B. Kajjam, K. Singh, S. Vaidyanathan, J. Mater. Chem. C 8 (2020) 11715–11726;
(d) R. Devi, K. Singh, S. Vaidyanathan, J. Mater. Chem. C 8 (2020) 8643–8653;
(e) R. Boddula, S. Vaidyanathan, Inorg. Chem. Acta 494 (2019) 141–153;
(f) R. Devi, S. Vaidyanathan, Dalton Trans. 49 (2020) 6205–6219;
(g) B. Rajamouli, P. Sood, S. Giri, V. Krishnan, V. Sivakumar, Eur. J. Inorg. Chem. 24 (2016) 3900–3911.
[31] (a) J. Andres, A.-S. Chauvin, In The rare earth elements: fundamentals and applications; D. A. Atwood, Ed.; Wiley: New York, 2012; pp. 606 (b) J. D. Routledge, M. W. Jones, S. Faulkner, M. Tropiano, Inorg. Chem. 54 (2015) 3337–334; (c) T. C. de Oliveira, H. P. Santos, M. G. Lahoud, D. F. Franco, R. O. Freire, J. D. L. Dutra, A. Cuin, J. F. de Lima, L. F. Marques, J. Lumin. 181 (2017) 196–210; (d) E. M. Gomes, D. F. Franco, S. L Scarpari, M. V. Colaço, M. S. Ferreira, R. O. Freire, L. F. Marques, J. Lumin. 210 (2019) 104-118.
[32] (a) G. Bobba, Y. Bretonnière, J.-C. Frias and D. Parker, Org. Biomol. Chem. 1 (2003) 1870–1872; (b) F. J. Steemers, W. Verboom, D. N. Reinhoudt, E. B. van der Tol, J. W. Verhoeven, J. Am. Chem. Soc. 117 (1995) 9408–9414; (c) C. Kachi-

Terajima, K. Yanagi, T. Kaziki, T. Kitazawaa, M. Hasegawa, Dalton Trans. 40 (2011) 2249–2256; (d) G. L. Law, T. A. Pham, J. D. Xu, K. N. Raymond, Angew. Chem., Int. Ed. 51 (2012) 2371–2374; (e) M. D. Regulacio, M. H. Pablico, J. A. Vasquez, P. N. Myers, S. Gentry, M. Prushan, S.-W. Tam-Chang, S. L. Stoll, Inorg. Chem. 47 (2008) 1512−1523; (f) Z. Ahmed, K. Iftikhar, J. Phys. Chem. A, 117 (2013) 11183−11201; (g) S. Shuvaev, V. Utochnikova, Ł. Marciniak, A. Freidzon, I. Sinev, R. V. Deun, R. O. Freire, Y. Zubavichus, W. Grünert, N. Kuzmina, Dalton Trans. 43 (2014) 3121–3136; (f) N. Kofod, R. Arppe-Tabbara, T. J. Sørensen, DOI: 10.1021/acs.jpca.8b12034.

[33] (a) J.C.G. Bünzli, A.S. Chauvin, H.K. Kim, E. Deiters, S.V. Eliseeva, Coord. Chem. Rev. 254 (2010) 2623–2633;
(b) D. Parker, Coord. Chem. Rev. 205 (2000) 109–130;
(c) T. Gunnlaugsson, J.P. Leonard, Chem. Commun. (2005) 3114–3131;
(d) K. Sénéchal-David, A. Hemeryck, N. Tancrez, L. Toupet, J.A.G. Williams, I. Ledoux, J. Zyss, A. Boucekkine, J.-P. Guégan, H.L. Bozec, O. Maury, J. Am. Chem. Soc. 128 (37) (2006) 12243–12255.

[34] (a) W.D.W. Horrocks Jr., D.R. Sudnick, J. Am. Chem. Soc. 101 (1979) 334–340;
(b) A. Beeby, I.M. Clarkson, R.S. Dickins, S. Faulkner, D. Parker, L. Royle, A.S. de Sousa, J.A.G. Williams, M. Woods, J. Chem. Soc. Perkin Trans. 1 (1999) 493–504.

[35] (a) D.J. Lewis, P.B. Glover, M.C. Solomons, Z. Pikramenou, J. Am. Chem. Soc. 133 (2011) 1033–1043;
(b) P.B. Glover, A.P. Bassett, P. Nockemann, B.M. Kariuki, R. Van Deun, Z. Pikramenou, Chem. Eur. J. 13 (2007) 6308–6320;
(c) Y. Haas, G. Stein, E.J. Wurzburg, Chem. Phys. 60 (1974) 258–263.

[36] G. Stein, E. Würzberg, J. Chem. Phys. 62 (1975) 208–213.

[37] A.C. Komor, J.K. Barton, Chem. Commun. 49 (2013) 3617–3630.

[38] T.M. Kelly, A.B. Tossi, D.J. McConnell, T.C. Strekas, Nucleic Acid Res. 13 (1985) 6017–6034.

[39] (a) A. Hussain, S. Gadadhar, T.K. Goswami, A.A. Karande, A.R. Chakravarty, Dalton Trans. 41 (2012) 885–895;
(b) A. Hussain, K. Somyajit, B. Banik, S. Banerjee, G. Nagaraju, A.R. Chakravarty, Dalton Trans. 42 (2013) 182–195;
(c) X. Liu, J. Xu, Y. Lv, W. Wu, W. Liu, Y. Tang, Dalton Trans. 42 (2013) 9840–9846;
(d) X. Wang, X. Wang, S. Cui, Y. Wang, G. Chen, Z. Guo, Chem. Sci. 4 (2013) 3748–3752.

[40] (a) R. Jastrza, M. Nowak, M. Skrobańska, A. Tolińska, M. Zabiszak, M. Gabryel, Ł. Marciniak, M.T. Kaczmarek, Coord. Chem. Rev. 382 (2019) 145–159;
(b) S. Shuvaev, M. Starck, D. Parker, Chem. Eur. J. 23 (2017) 9974–9989.

[41] (a) P.B. Glover, P.R. Ashton, L.J. Childs, A. Rodger, M. Kercher, R.M. Williams, L. D. Cola, Z. Pikramenou, J. Am. Chem. Soc. 125 (2003) 9918–9919;
(b) E.L. Crossley, J.B. Aitken, S. Vogt, H.H. Harris, L.M. Rendina, Angew. Chem. Int. Ed. 49 (2010) 1231–1233.

[42] (a) M.J. Waring, J. Mol. Biol. 13 (1965) 269–282;
(b) D.L. Boger, B.E. Fink, S.R. Brunnette, W.C. Tse, M.P. Hedrick, J. Am. Chem. Soc. 123 (2001) 5878–5891.

[43] N.S. Quiming, R.B. Vergel, M.G. Nicolas, J.A. Villanueva, J. Health Sci. 51 (2005) 8–15.

[44] (a) A. Sulkowska, J. Mol. Struct. 616 (2002) 227–232;
(b) D. Voet, Biochemistry, John Wiley & Sons, Inc, 3rd edn, 1995;
(c) J.R. Lakowicz, G. Webber, Biochemistry 12 (1973) 4161–4170;
(d) J. Ghuman, P.A. Zunszain, I. Petitpas, A.A. Bhattacharya, M. Otagiri, S. Curry, J. Mol. Biol. 353 (2005) 38–52.

[45] J.R. Lakowicz, Principles of Fluorescence Spectroscopy, third ed., Springer, New York, 2006.

[46] (a) J.N. Miller, Proc. Anal. Div. Chem. Soc. 16 (1979) 203–208;
(b) Y.J. Hu, Y. Liu, Z.B. Pi, S.S. Qu, Bioorg. Med. Chem. 13 (2005) 6609–6614;
(c) J.H. Tang, F. Luan, X.G. Chen, Bioorg. Med. Chem. 49 (2006) 3210–3217.

[47] (a) J. Yu, D. Parker, R. Pal, R.A. Poole, M.J. Cann, J. Am. Chem. Soc. 128 (2006) 2294–2299;
(b) S.J. Butler, B.K. McMahon, R. Pal, D. Parker, J.W. Walton, Chem. Eur. J. 19 (2013) 9511–9517;
(c) E. Deiters, B. Song, A.-S. Chauvin, C.D.B. Vandevyver, F. Gumy, J.-C.G. Bünzli, Chem. Eur. J. 15 (2009) 885–900.

[48] (a) V. Divya, M.L.P. Reddy, R. Pavithran, Dalton Trans. 42 (2013) 15249–15262;
(b) V. Divya, V. Sankar, K.G. Raghu, M.L.P. Reddy, Dalton Trans. 42 (2013) 12317–12323;
(c) T.M. George, M.S. Krishna, M.L.P. Reddy, Dalton Trans. 45 (2016) 18719–18729.

[49] (a) S. Monro, K.L. Colón, H. Yin, J. Roque, P. Konda, S. Gujar, R.P. Thummel, L. Lilge, C.G. Cameron, S.A. McFarland, Chem. Rev. 119 (2019) 797–828;
(b) G.-L. Law, R. Pal, L.O. Palsson, D. Parker, K.-L. Wong, Chem. Commun. (2009) 7321–7323;
(c) J.-X. Zhang, H. Li, C.-F. Chan, R. Lan, W.-L. Chan, G.-L. Law, W.-K. Wong, K.-L. Wong, Chem. Commun. 48 (2012) 9646–9648;
(d) A. de Bettencourt-Dias, K.R. Johnson, S.B. Vittardi, M.A. Gracia-Nava, J. J. Rack 26 (2020) 7274–7280.

[50] (a) W.Y. Ng, X. Gong, W.K. Chan, Chem. Mater. 11 (1999) 1165–1170;
(b) C. Zhang, Z.-M. Huo, T.-T. Wang, H.-P. Zeng, J. Phys. Org. Chem. 25 (2012) 754–759.

[51] APEX2 v2012.4, Bruker AXS: Madison, WI, 1999.

[52] (a) G. M. Sheldrick, SADABS 2.0; University of Göttingen: Göttingen, Germany, 2000; (b) G. M. Sheldrick, SADABS, Area Detector Absorption Correction, University of Göttingen, Göttingen, Germany, 2001.

[53] (a) G.M. Sheldrick, SHELXL-2014: Program for Crystal Structure Refinement, University of Göttingen, Göttingen, Germany, 2014;
(b) G.M. Sheldrick, Acta Crystallogr. C 71 (2015) 3–8.

[54] O.V. Dolomanov, L.J. Bourhis, R.J. Gildea, J.A.K. Howard, H. Puschmann, OLEX2: A complete structure solution, refinement and analysis program, J. Appl. Cryst. 42 (2009) 339–341.

[55] M.N. Burnett, C.K. Johnson, ORTEP-III, Report ORNL - 6895, Oak Ridge, TN, Oak Ridge National Laboratory, 1996.

[56] (a) J. Marmur, J. Mol. Biol. 3 (1961) 208–218;
(b) M.E. Reichmann, C.A. Rice, C.A. Thomas, P. Doty, J. Am. Chem. Soc. 76 (1954) 3047–3053.

[57] (a) A. Wolfe, G.H. Shimer Jr., T. Meehan, Biochemistry 26 (1987) 6392–6396;
(b) D.E.V. Schmechel, D.M. Crothers, Biopolymers 10 (1971) 465–480.

[58] (a) M. Lee, A.L. Rhodes, M.D. Wyatt, S. Forrow, J.A. Hartley, Biochemistry 32 (1993) 4237–4245;
(b) A.R. Morgan, J.S. Lee, D.E. Pulleyblank, N.L. Murray, D.H. Evans, Nucleic Acids Res. 7 (1979) 547–569;
(c) F.J. Meyer-Almes, D. Porschke, Biochemistry 32 (1993) 4246–4253;
(d) F.D. Abreu, T.F. Paulo, M.H. Gehlen, R.A. Ando, L.G.F. Lopes, A.C.S. Gondim, M.A. Vasconcelos, E.H. Teixeria, E.H.S. Sousa, I.M.M. de Carvalho, Inorg. Chem. 56 (2017) 9084–9096.

[59] G. Scatchard, Ann. N. Y. Acad. Sci. 51 (1949) 660–672.

[60] (a) P. Qu, H. Lu, X. Ding, Y. Tao, Z. Lu, J. Mol. Struct. 920 (2009) 172–177;
(b) Y.-Q. Wang, H.-M. Zhang, Q.-H. Zhou, J. Mol. Struct. 932 (2009) 31–37;
(c) R.G. Machicote, M.E. Pacheco, L. Bruzzone, Spectrochim. Acta A 78 (2011) 1535–1539.